

Contract No:

This document was prepared in conjunction with work accomplished under Contract No. DE-AC09-08SR22470 with the U.S. Department of Energy (DOE) Office of Environmental Management (EM).

Disclaimer:

This work was prepared under an agreement with and funded by the U.S. Government. Neither the U. S. Government or its employees, nor any of its contractors, subcontractors or their employees, makes any express or implied:

- 1) warranty or assumes any legal liability for the accuracy, completeness, or for the use or results of such use of any information, product, or process disclosed; or
- 2) representation that such use or results of such use would not infringe privately owned rights; or
- 3) endorsement or recommendation of any specifically identified commercial product, process, or service.

Any views and opinions of authors expressed in this work do not necessarily state or reflect those of the United States Government, or its contractors, or subcontractors.

***Crack Growth Rate and Large
Plate Demonstration of Chloride-
induced Stress Corrosion
Cracking in Spent Nuclear Fuel
Storage Canisters***

Spent Fuel and Waste Disposition

***Prepared for
U.S. Department of Energy
Spent Fuel and Waste Science and Technology***

***Poh-Sang Lam
Andrew J. Duncan
Robert L. Sindelar
Savannah River National Laboratory***

September 30, 2019
Milestone No. M3SF-19SR010201052
SRNL-STI-2019-00561

DISCLAIMER

This information was prepared as an account of work sponsored by an agency of the U.S. Government. Neither the U.S. Government nor any agency thereof, nor any of their employees, makes any warranty, expressed or implied, or assumes any legal liability or responsibility for the accuracy, completeness, or usefulness, of any information, apparatus, product, or process disclosed, or represents that its use would not infringe privately owned rights. References herein to any specific commercial product, process, or service by trade name, trade mark, manufacturer, or otherwise, does not necessarily constitute or imply its endorsement, recommendation, or favoring by the U.S. Government or any agency thereof. The views and opinions of authors expressed herein do not necessarily state or reflect those of the U.S. Government or any agency thereof.

Prepared by
Savannah River National Laboratory
Savannah River Nuclear Solutions
Aiken, South Carolina 29808

Savannah River National Laboratory is a multiprogram laboratory managed and operated by Savannah River Nuclear Solutions, LLC, for the U.S. Department of Energy under contract DE-AC09-09SR22505.



EXECUTIVE SUMMARY

This report describes the body of work involving testing and analyses performed in FY18 and FY19 at the Savannah River National Laboratory and at Korea University to determine chloride-induced stress corrosion crack (CISCC) growth rates in weldments of austenitic stainless steel plate material. The primary work involved:

- several separate crack growth rate test campaigns with new testing setups using laboratory-scale corrosion specimens;
- analyses to estimate the stress intensity factors for flaws postulated to be present in the residual stress fields of axial and circumferential weldments in a prototypic dry storage canister; and
- establishment of a “large plate” (approximately 51×46 cm with thickness 16 mm and weight about 30 kg) CISCC test that uses a plate with a circumferential weldment harvested from the Sandia National Laboratories’ full-size mockup dry storage canister.

The tests for crack growth rate were conducted on ASTM E1861 bolt-load compact tension specimens in a setup designed to allow initially dried salt deposits to deliquesce and infuse the brine to the crack front under conditions relevant to the canister storage environments (e.g., temperature and humidity). The crack growth rate test results matched previous experimental data in the open literature. These literature data had been compiled by SNL and EPRI to develop a temperature-dependent (K-insensitive) crack growth rate model to support flaw disposition in the ASME Boiler and Pressure Vessel Section XI Code Case N-860, “Examination Requirements and Acceptance Standards for Spent Nuclear Fuel Storage and Transportation Containment Systems.”

The knowledge of the salt, temperature, humidity conditions for CISCC including the threshold stress intensity factor, K_{ISCC} , were used to setup the large plate test in which a set of part-through-wall and through-wall electrical discharge machined (EDM) defects were positioned in the weld residual stress field of the welded plate material from the mockup canister. A salt solution was applied to this plate specimen with an air-brush spray, then dried, and then exposed to a constant 75% RH condition at an ambient room temperature of 22 °C. The salt loading and environmental condition is expected to be aggressive to cause CISCC. The visual results at the surface of the plate show corrosion product staining (brown rust appearance) but with no CISCC emanating from the machined notches after approximately 5 months exposure to date.

The plate test will continue in FY20 and phased-array ultrasonic testing and other NDE techniques will be applied to identify and characterize CISCC that may emanate from the machined defects. The notches and any CISCC from them will be sectioned at the conclusion of the test to verify NDE characterization, and to develop effective through-wall crack growth rates from cracks that would likely be branched.

This report fulfills the M3 milestone M3SF-19SR010201052, “Summary Report of Canister Corrosion Testing” under Work Package Number SF-19SR01020105.

ACKNOWLEDGMENTS

The authors gratefully acknowledge the support of Ned Larson, U.S. Department of Energy, Office of Nuclear Energy, Office of Spent Fuel and Waste Disposition, Office of Spent Fuel & Waste Science and Technology, for his office's sponsorship of this work, including the collaboration with Korea University under the I-NERI program. The authors thank the corrosion expert staff from Sandia National Laboratories (Charles Bryan, Eric Schindelholz) and the Pacific Northwest National Laboratory (Mychailo Toloczko) for helpful discussions throughout the course of this work. The authors thank John Kessler, of John Kessler Associates, for his thorough read to improve the quality of this document.

The authors are grateful for the consultation and advice from our colleagues at the Savannah River National Laboratory, Bruce Wiersma, John Mickalonis, and Brenda Garcia-Diaz. The authors give a special acknowledgment to Lisa Ward and Kellie Holland for their laboratory work in this project.

The authors give an extra special acknowledgment to our partners at Korea University (Seoul, Republic of Korea), Professor Yun-Jae Kim and his students, for their companion work and supporting analyses.

CONTENTS

EXECUTIVE SUMMARY iii

ACKNOWLEDGMENTS iv

LIST OF FIGURES vi

LIST OF TABLES ix

ACRONYMS xi

1. INTRODUCTION 1

2. CRACK GROWTH RATE TESTS 2

 2.1 Instrumented Bolt-load Compact Tension Specimen 5

 2.2 Crack Growth Rate Test with Mixture of Salt and Dust 8

 2.2.1 Experiment 8

 2.2.2 Results 12

 2.3 Crack Growth Rate Test with Dry Salt 14

 2.3.1 Experiment 15

 2.3.2 Results 19

 2.4 I-NERI: Korea University Compact Tension Test for CISCC 21

 2.4.1 Experiment 21

 2.4.2 Results 24

3. COMPANION TEARDROP SPECIMENS 26

 3.1 Experimental Observation and Characterization 26

 3.2 Additional Artificial Sea Salt Testing 31

4. LARGE PLATE DEMONSTRATION OF CISCC 34

 4.1 Starter Cracks 34

 4.2 Experiment 37

 4.3 Experimental Observation 38

 4.4 Calculation of Stress Intensity Factors for Starter Cracks in Large Plate 40

5. CONCLUDING REMARKS 45

6. REFERENCES 46

LIST OF FIGURES

Figure 1. Criterion of stress corrosion cracking 3

Figure 2. Dependence of crack growth rate (da/dt) on stress intensity factor (K_I is the Mode I stress intensity factor, K_{ISCC} is the threshold for stress corrosion cracking, and K_{IC} is the fracture toughness of the material) 3

Figure 3. Pre-cracked specimen geometries for stress corrosion testing (Courtesy of Naval Research Laboratory, Washington, DC) [27] 4

Figure 4. ASTM E1681 bolt loaded compact tension specimen design with 10% side groove on each side of the specimen 5

Figure 5. Expected crack growth behavior of “falling K ” constant displacement CT test..... 6

Figure 6. Instrumented bolt design..... 7

Figure 7. Typical load - time response of instrumented bolt..... 8

Figure 8. Schematic arrangement of the bolt-load CT specimen in constant humidity vessel that is placed inside an oven with constant temperature 10

Figure 9. Teardrop coupon used to provide convenient assessment of the bolt-load CT specimen during CISCC test 11

Figure 10. SCC test configuration showing the cradled instrumented bolt-load CT (BLCT) specimen and a companion teardrop coupon in a constant humidity vessel 11

Figure 11. Experimental set up for CGR test using three different salt/dust mixtures and RH conditions at a constant oven temperature 12

Figure 12. Specimens as removed from test cells..... 13

Figure 13. Optical and SEM images of the fracture surface of the bolt-load CT specimen (Specimen 1) exposed to simulated calcium-rich salt at 50 °C and 50% RH for 5 months..... 14

Figure 14. The Bolt-Load CT specimens as machined from two plates cut from the mockup canister..... 16

Figure 15. The WRS Components RS3 (Perpendicular to Circumferential Weld) and RS4 Parallel to the Axial Weld) [15,32] (Courtesy of Korea University under I-NERI/USA-ROK) 16

Figure 16. Typical configuration of the bolt-load CT specimen packed with dry salt (a) and then installed in a closed glass vessel with teardrop coupon under constant humidity condition (b) 17

Figure 17. Cellulose wicks (in vendor package and in a test tray with water drops) used to transport deliquescing salt to crack front in bolt-load CT specimens 18

Figure 18. Typical fracture surface under CISCC 19

Figure 19. Chloride-induced stress corrosion crack growth rates under wide range of exposure conditions (original figure courtesy of Sandia National Laboratories [17-19]) 21

Figure 20. Schematic diagram of the CGR test apparatus with standard CT specimen..... 22

Figure 21. Standard compact tension specimen as recommended by ASTM E1820..... 23

Figure 22. Korea University CISCC test conducted in an environmental control chamber 23

Figure 23. Typical fracture surface of CT specimen at KU with SCC indicated by arrows in the inset (Courtesy of Korea University under I-NERI/USA-ROK) 24

Figure 24. Dependence of crack growth rate (da/dt) on stress intensity factor (K) 25

Figure 25. The location of maximum stress in the tear drop specimen [29,30] 26

Figure 26. Adherent dust on teardrop Sample No. 1 following test (a) and the post-cleaning image with outlined corrosion region (b) 27

**Crack Growth Rate and Large Plate Demonstration of Chloride-induced Stress Corrosion
Cracking in Spent Nuclear Fuel Storage Canisters**

September 30, 2019

vii

Figure 27. Image of the corrosion region on Sample 1..... 27

Figure 28. The LCM images of Area 1 in the corrosion area and the linear profiles of the cross-sections along Lines A and B, respectively 28

Figure 29. The LCM images of Area 2 in the corrosion area..... 28

Figure 30. Images of cross-section B in Area 1 show transgranular stress corrosion cracks and pitting corrosion 29

Figure 31. Images of the cross-section in Area 2 show transgranular stress corrosion cracks and pitting corrosion 29

Figure 32. Characterization of pits and the associated stress corrosion cracks in sectioned teardrop coupon Sample 1..... 30

Figure 33. Relationship between pit depth and the associated crack depth (symbol \blacklozenge) as well as the corresponding crack growth rate (symbol \times) as converted from crack depth averaged by test duration (5 months) 31

Figure 34. LCM images of cracking initiated on the surface of teardrop coupons at 50 °C and 50% RH for 100% sea salt (a), 25% sea salt + 75% CeO₂ (b), and at autogenous weld interface (shown by a dark line) in 25% sea salt + 75% artificial dust (c) 32

Figure 35. Composite image showing pitting/cracking at various locations in teardrop coupons exposed to dehydrated sea salt after 3-month exposure at 50 °C and 50% RH 33

Figure 36. Large plate cut from a canister with an as-fabricated circumferential weld and the locations of starter cracks for CISCC test..... 35

Figure 37. Large plate starter crack configurations: (a) VT1, VT2: through-wall crack across the weld; (b) HT1: through-wall crack parallel to the weld edge; (c) VP1, VP2, VP3: semi-circular part-through-wall crack perpendicular to the weld edge; (d) HP1: semi-circular part-through-wall crack parallel to the weld edge 36

Figure 38. Large plate starter crack design as viewed from plate cross-section through the circumferential weld (superimposed over the contour map for welding residual stress parallel to the weld [15]) 36

Figure 39. Large plate with EDM starter cracks after salt spray and drying 37

Figure 40. Phased array ultrasonic test (PAUT) for on-line monitoring of CISCC in the large plate with 7 EDM starter cracks 38

Figure 41. Experimental setup of the large plate CISCC test under naturally deliquescing sea salt at room temperature and 75% RH 38

Figure 42. Deliquescence occurred in hours and forming numerous liquid droplets 39

Figure 43. Stainless steel coupons used to verify deliquescence phenomenon..... 39

Figure 44. Layout and designations of EDM starter cracks (a) and evolution of chloride-induced corrosion near these cracks (b) during 3-month exposure at room temperature and 75% RH..... 40

Figure 45. Curve-fitting of the welding residual stresses at weld centerline and at heat affected zone: WRS parallel to the circumferential weld: RS2; $x= 0$ at the canister inner surface (Courtesy of Korea University under I-NERI/USA-ROK) 41

Figure 46. Curve-fitting of the welding residual stresses at weld centerline and at heat affected zone: WRS parallel to the circumferential weld: RS2; $x= 0$ at the canister outer surface (Courtesy of Korea University under I-NERI/USA-ROK) 42

**Crack Growth Rate and Large Plate Demonstration of Chloride-induced Stress Corrosion
Cracking in Spent Nuclear Fuel Storage Canisters**

Figure 47. Curve-fitting of the welding residual stresses at weld centerline and at heat affected zone:
WRS perpendicular to the circumferential weld: RS3; $x=0$ at the canister inner surface (Courtesy of
Korea University under I-NERI/USA-ROK)..... 42

Figure 48. Curve-fitting of the welding residual stresses at weld centerline and at heat affected zone:
WRS parallel to the circumferential weld: RS3; $x=0$ at the canister outer surface (Courtesy of Korea
University under I-NERI/USA-ROK) 43

Figure 49. Stress intensity factors of the starter cracks in the residual stress fields for a circumferential
weld in the mockup canister..... 43

Figure 50. Summary of crack growth rate field test data obtained on Miyakojima Island [4] (Courtesy of
Korea University under I-NERI/USA-ROK)..... 45

LIST OF TABLES

Table 1..Experimental conditions of exposure in dry salt crack growth testing..... 9

Table 2. Material Chemical Composition for Sandia mockup canister (wt.%) [15] 15

Table 3. Crack growth rate test matrix using bolt-load CT specimens 18

Table 4. Results of bolt-load CT tests up to six months 20

Table 5. Chemical compositions of 304 stainless steel (wt.%) – Korea University 22

Table 6. . Summary of CISCC test results from Korea University [21,22] (304 stainless steel immersed in a chloride solution with 5 % salinity at 50 °C)..... 25

Table 7. Stress Intensity factors for starter cracks VP1, VP2, and VP3 (Axial surface crack: $a = c = 6$ mm; semicircular)..... 44

Table 8. Stress Intensity factors for starter cracks VT1 and VT2 (Axial through-wall crack: $c = 12.5$ mm) 44

Table 9. Stress Intensity factors for starter crack HP1 (Circumferential surface crack: $a = c = 6$ mm; semicircular)..... 44

Table 10. Stress Intensity factors for starter cracks HT1 (Circumferential through-wall crack: $c = 12$ mm; semicircular)..... 44

**Crack Growth Rate and Large Plate Demonstration of Chloride-induced Stress Corrosion
Cracking in Spent Nuclear Fuel Storage Canisters**

September 30, 2019

x

This page is intentionally left blank

ACRONYMS

AMP	Aging Management Program
API	American Petroleum Institute
ASME	American Society of Mechanical Engineers
BLCT	Bolt-load Compact Tension (specimen)
BM	Base metal
BPVC	Boiler and Pressure Vessel Code
CISCC	Chloride-Induced Stress Corrosion Cracking
CGR	Crack Growth Rate
COD	Crack opening displacement
CRIEPI	Central Research Institute of Electric Power Industry (Japan)
CT	Compact Tension Specimen
DAS	Data acquisition system
DOE	US Department of Energy
EDM	Electrical Discharge Machining
EPRI	Electric Power Research Institute
HAZ	Heat Affected Zone
ISFSI	Independent Spent Fuel Storage Installation
I-NERI	International Nuclear Energy Research Initiative
KU	Korea University
LWR	Light Water Reactor
NDE	Nondestructive Examination
NE	Nuclear Energy
NRC	Nuclear Regulatory Commission
PAUT	Phased Array Ultrasonic Test
PNNL	Pacific Northwest National Laboratory
RH	Relative Humidity
SAW	Submerged arc welding
SCC	Stress Corrosion Cracking
SIF	Stress Intensity Factor
SNF	Spent Nuclear Fuel

**Crack Growth Rate and Large Plate Demonstration of Chloride-induced Stress Corrosion
Cracking in Spent Nuclear Fuel Storage Canisters**

xii

September 30, 2019

SNL	Sandia National Laboratories
SRNL	Savannah River National Laboratory
UT	Ultrasonic Test
WRS	Welding Residual Stress

1. INTRODUCTION

Nearly 3000 spent nuclear fuel (SNF) dry storage canisters are currently in the Independent Spent Fuel Storage Installations (ISFSIs) in the United States. Because the canisters are not required to be stress relieved after welding and fabrication, stress corrosion cracking (SCC) has been identified as a potential concern due to the possibility of through-wall penetration that could breach the confinement boundary provided by the canisters. For canisters at ISFSIs near coastal regions, chloride-bearing salts may deposit on the external surface of the canister. Typically, the heat from radioactive decay at the time the dry storage canisters were loaded with SNF provides a canister with sufficient thermal mass to maintain the surface temperatures above the temperatures that allow deliquescence of atmospheric salts to occur¹, thereby limiting the occurrence of the surface brine, which is essential for the onset of chloride-induced stress corrosion cracking (CISCC). As canisters cool, surface temperatures will drop below this threshold in the long-term storage. If the local relative humidity at the canister surface is high enough, salt deposits may deliquesce and form aggressive brine. With the welding residual stress (WRS) as the driving force, CISCC may take place in the weldment and/or the heat affected zone (HAZ) in these canisters.

As dictated by the aging management program (AMP), which is required for relicensing applications [1], canister inservice inspection is to be performed. The U. S. Nuclear Regulatory Commission (NRC) requested the Section XI committee of the American Society of Mechanical Engineers (ASME) Boiler and Pressure Vessel Code (BPVC) to provide the requirements for inspection, and Code Case N-860, entitled “Examination Requirements and Acceptance Standards for Spent Nuclear Fuel Storage and Transportation Containment Systems” was undertaken. The code case includes inspection, flaw acceptance standards, and corrosion assessment to manage the potential CISCC degradation. The Code Case N-860 has been under development since 2015 and issuance is expected in 2020.

An important element of Code Case N-860 is to provide guidance on flaw disposition. This would require an assignment of a crack growth rate (CGR) [2] should a flaw be detected and determined to be due to CISCC. Many CISCC tests under marine environments or various brine conditions have been conducted for several years, notably done by the work at Central Research Institute of Electric Power Industry (CRIEPI) in Japan [3-10].

This report describes the development of CISCC tests at Savannah River National Laboratory (SRNL) [11-14]. These tests utilize the deliquescent nature of salts under certain temperature and humidity conditions. The following paragraphs provide a brief summary of the testing that was done. Additional details of the specific test conditions are provided in the original references, and in the body of this report.

The instrumented bolt-load compact tension (CT) fracture mechanics specimens have been used for more accurate measurement of CGR. The initial set of bolt-load CT specimens, used to

¹ For actual deliquescence, a temperature between 50 to 55 °C is the maximum possible. However, at 15% RH where SCC has been observed experimentally, the maximum temperature is in the range of 65-70°C.

evaluate the salt/dust constituent effects, were machined from 304 stainless steel plates. These archival (pre-1980) plates had a “high” carbon content, with 0.063 wt.% C [11,12]. More recently a set of bolt-load CT specimens [13, 14] were harvested from two plates cut from a dual certified 304/304L stainless steel mockup canister [15]; one of the plates contains an axial weld and the other a circumferential weld. These CT specimens were machined from the base metal (BM) and from the HAZ. The specimens were packed with dry salt and under the exposure conditions targeted at 22 and 37 °C with relative humidity (RH) 75% for 2 and 6 months. Stress corrosion cracks were observed in some specimens. The estimated CGRs are consistent with the general data trend from a collection of historical test data under various exposure conditions [16-19].

A parallel CISCC testing has been developed at Korea University (KU) under the U. S. Department of Energy (DOE) International Nuclear Energy Research Initiative (I-NERI) between the United States (SRNL) and the Republic of Korea (KU) [20]. Standard CT specimens at KU were loaded with a custom-designed load cell and were immersed in solution with 5% salinity at 50 °C [21, 22]. A consistent CGR was obtained from each of their test.

A companion teardrop coupon (304L stainless steel) is usually placed next to the bolt-load CT specimen in the SRNL environmental test cell to provide a convenient assessment for general corrosion and cracking but is not designed for CGR measurement. Detailed metallographic examinations were performed in the pitting and cracking areas after exposure [12-14, 23]. The results could not establish a correlation between the pit size and crack depth (length).

As a long-term demonstration of CISCC driven by WRS, a large section (approximately 51×46 cm with thickness 16 mm and weight about 30 kg), which contains a circumferential weld, was cut from the mockup canister [15]. Through-wall and part-through-wall (surface) starter cracks, either parallel or perpendicular to the weld, were fabricated with electrical discharge machining (EDM). The stress intensity factor (K) for each machined starter crack under canister welding residual stress was estimated by the American Petroleum Institute (API) 579 procedure [24,25]. Dry salt was applied over these machined cracks (estimated 2.35 g/m² chloride) and natural deliquescence was allowed to take place at room temperature and 75% RH [14]. Phased array ultrasonic test (PAUT) transducers and probes were deployed on the plate intended for on-line detection of the CISCC events. Other nondestructive examination (NDE) techniques are also planned to evaluate CISCC on this plate. The large plate test has been on-going since May 2019, no CISCC has been observed but the evolution of general corrosion near the starter cracks is monitored and documented.

2. CRACK GROWTH RATE TESTS

In a sufficiently aggressive environment, if the material (metal) is susceptible to SCC and a sufficient loading is present to sustain SCC, then SCC will take place (Figure 1). In fracture mechanics the loading is characterized by stress intensity factor (K) for a cracked body. When $K_{applied} > K_{ISCC}$, the load criterion for SCC is met for that material in a specific environment, where $K_{applied}$ is the applied stress intensity factor due to external and internal loads, and K_{ISCC} is

the threshold Mode I (opening mode) stress intensity factor (denoted by K_I). Note that K_{ISCC} is considered as a material property for a material under certain environmental conditions, below which SCC cannot occur. Phenomenologically, stress corrosion cracking typically has a dependency on $K_{applied}$ (or denoted by K_I for short) as shown in Figure 2, where Phase I represents the SCC initiation stage, Phase II is the primary SCC growth regime, and Phase III is the region where catastrophic failure would occur.

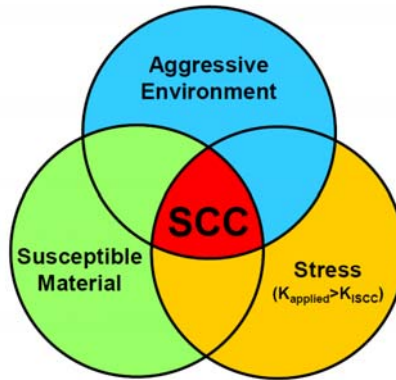


Figure 1. Criterion of stress corrosion cracking

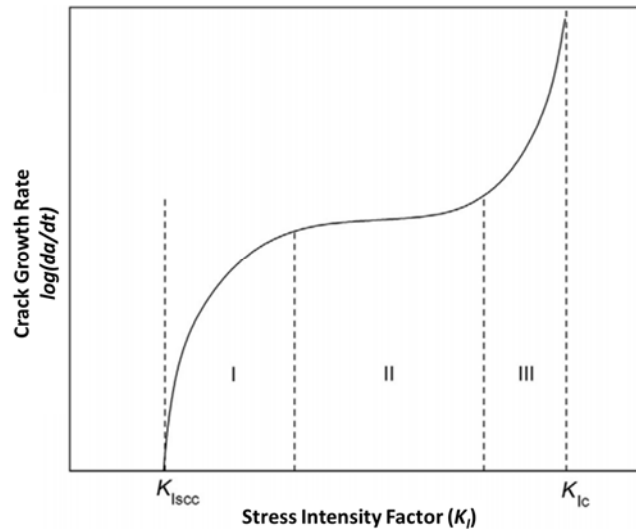


Figure 2. Dependence of crack growth rate (da/dt) on stress intensity factor (K_I is the Mode I stress intensity factor, K_{ISCC} is the threshold for stress corrosion cracking, and K_{IC} is the fracture toughness of the material)

Appendix C of the ASME BPVC Section XI [26] provides guidance for evaluation of SCC growth rate in light-water reactor (LWR) conditions. In Appendix C Article C-8500, a general expression for CGR (da/dt) is given:

$$\frac{da}{dt} = \exp \left[-\frac{Q_g}{R_g} \left(\frac{1}{T_{abs}} - \frac{1}{T_{ref}} \right) \right] \phi(K_I - K_{ISCC})^\eta \quad (1)$$

where Q_g is the thermal activation energy for SCC, R_g the universal gas constant, T_{abs} the absolute metal operating temperature, T_{ref} the absolute reference temperature, ϕ the CGR coefficient, and η the CGR exponent.

Stress corrosion cracking experiments under CISCC conditions have been carried out. Theoretically, the CGR test data are fitted into Eq. (1) as a prediction tool to establish flaw re-examination intervals should flaws be detected on the canister. Figure 3 shows various geometries and loading modes for CGR test specimens, which were proposed by U. S. Naval Research Laboratory [27]. From Figure 3, the constant displacement, decreasing K , wedge opening loaded (WOL) compact tension specimen was selected for CISC testing at SRNL (i.e., bolt-load CT specimen).

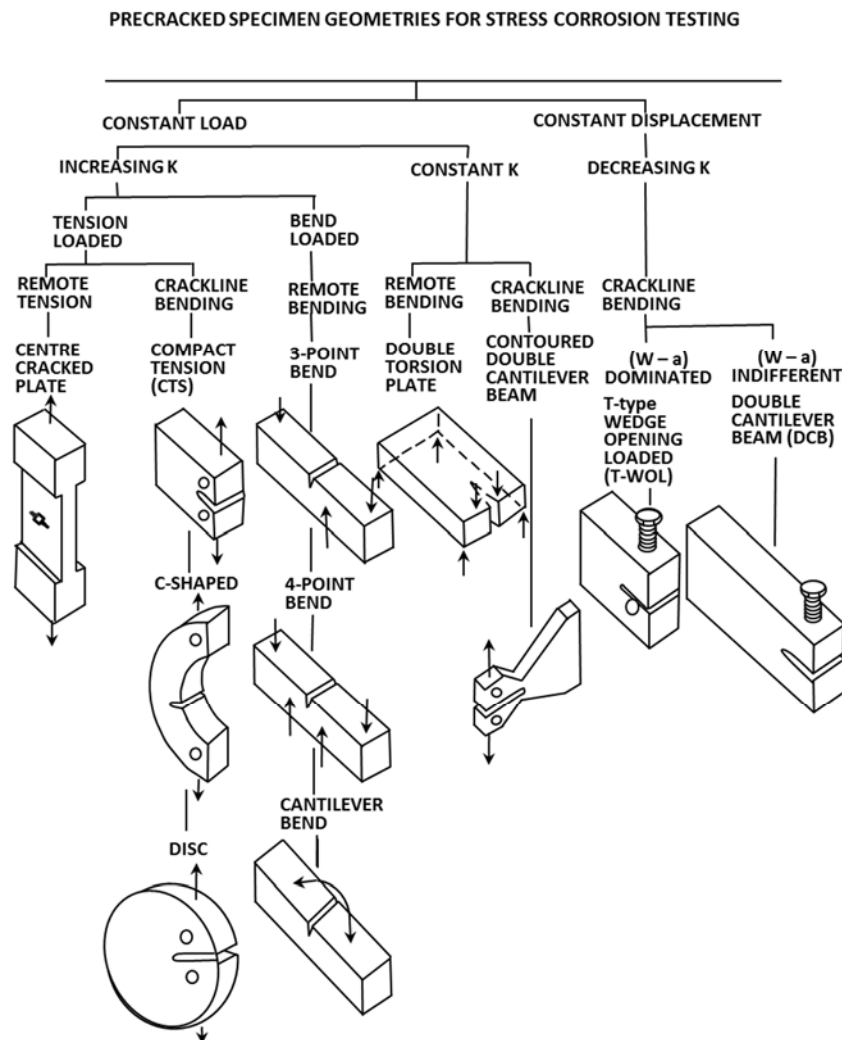


Figure 3. Pre-cracked specimen geometries for stress corrosion testing (Courtesy of Naval Research Laboratory, Washington, DC) [27]

2.1 Instrumented Bolt-load Compact Tension Specimen

The bolt-load compact tension specimens used for SRNL testing were either machined from archival 304 stainless steel plates (Section 2.2) or from plates cut from a dual certified 304/304L stainless steel full-size mockup canister (Section 2.3). The specimen design, as shown in Figure 4, is based on ASTM E1681 “*Standard Test Method for Determining Threshold Stress Intensity Factor for Environment-Assisted Cracking of Metallic Materials.*” The width (W) between the bolt centerline and the back plane is 25 mm, the total height ($2H$) is 25 mm, and the thickness (B) 12.7 mm with 10% side groove on each side [11-14].

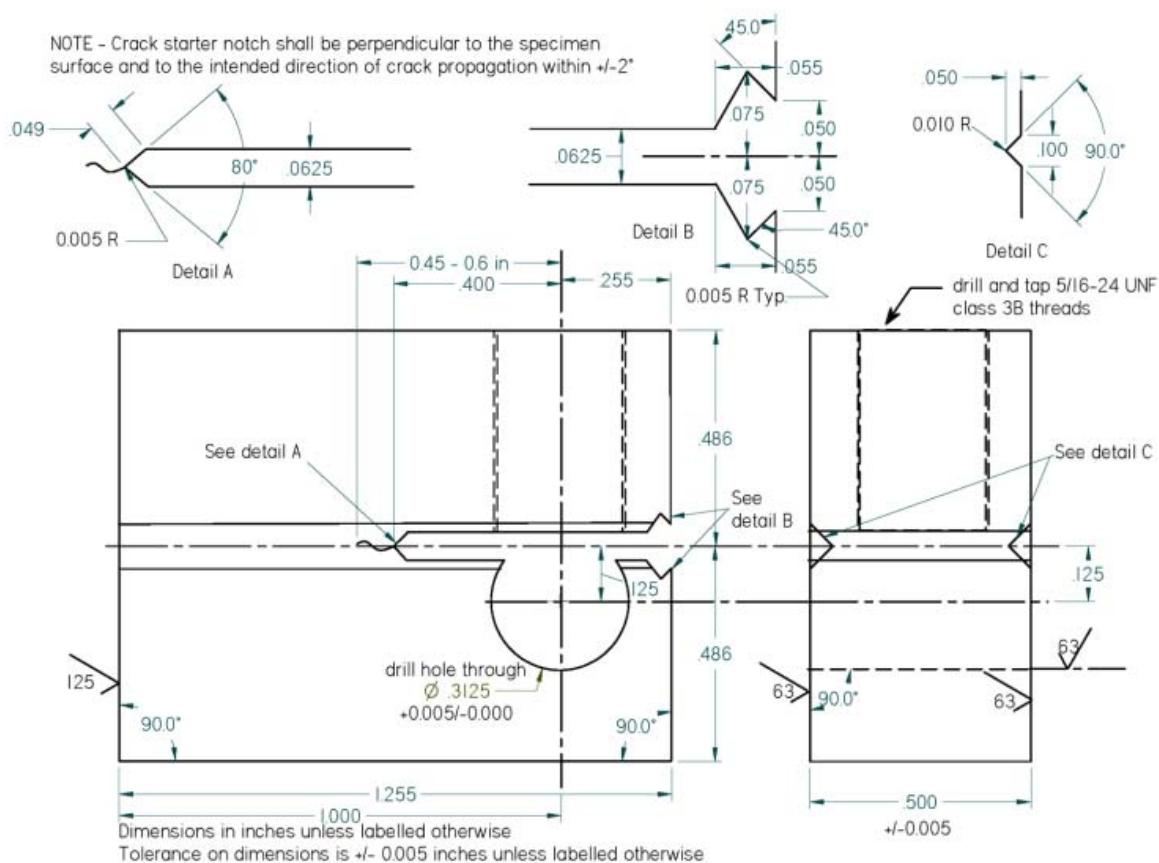


Figure 4. ASTM E1681 bolt loaded compact tension specimen design with 10% side groove on each side of the specimen

Pre-cracks were initiated in the specimen by fatigue in air to produce a naturally sharp crack tip so the total initial crack length between 12 to 15 mm (or $a/W = 0.5$ to 0.6) could be obtained to meet the requirement of ASTM E1681. Fatigue cracking was conducted at stress intensity factors as low as possible (~ 5 - 10 MPa \sqrt{m}) consistent with developing a crack in the specimens

within 24 hours. The specimens were cleaned in isopropanol and dried. The cleaned specimens were then loaded to desired stress intensity factors. This was achieved by first elastically loading and unloading specimens in an Instron 4507 mechanical testing machine while recording load and crack opening-displacement (COD). The specimens were then reloaded in a vice with an instrumented bolt to a COD value corresponding to the desired stress intensity factor.

The stress intensity factor, K , is determined for the crack front (crack tip) per Equation 4 in ASTM E1681, which is dependent on crack length (a), elastic modulus (E), crack mouth opening displacement (COD), and the specimen width (W). The bolt-load CT test is conducted under “falling K ” kinetics that would allow for the examination of the relationship between K and crack growth rate (da/dt), as well as, provide data to determine a threshold value for stress corrosion cracking (K_{ISCC}), if it exists (see Figure 5). The arrows in Figure 5 illustrate the relationship between K and a/W for a COD values used in this test. As the crack grows, K drops until the CGR stops. This K level is referred to as K_{ISCC} . The CT specimens were loaded to approximately $33 \text{ MPa}\sqrt{\text{m}}$, the maximum possible per guidance in the standard to avoid plasticity effects.

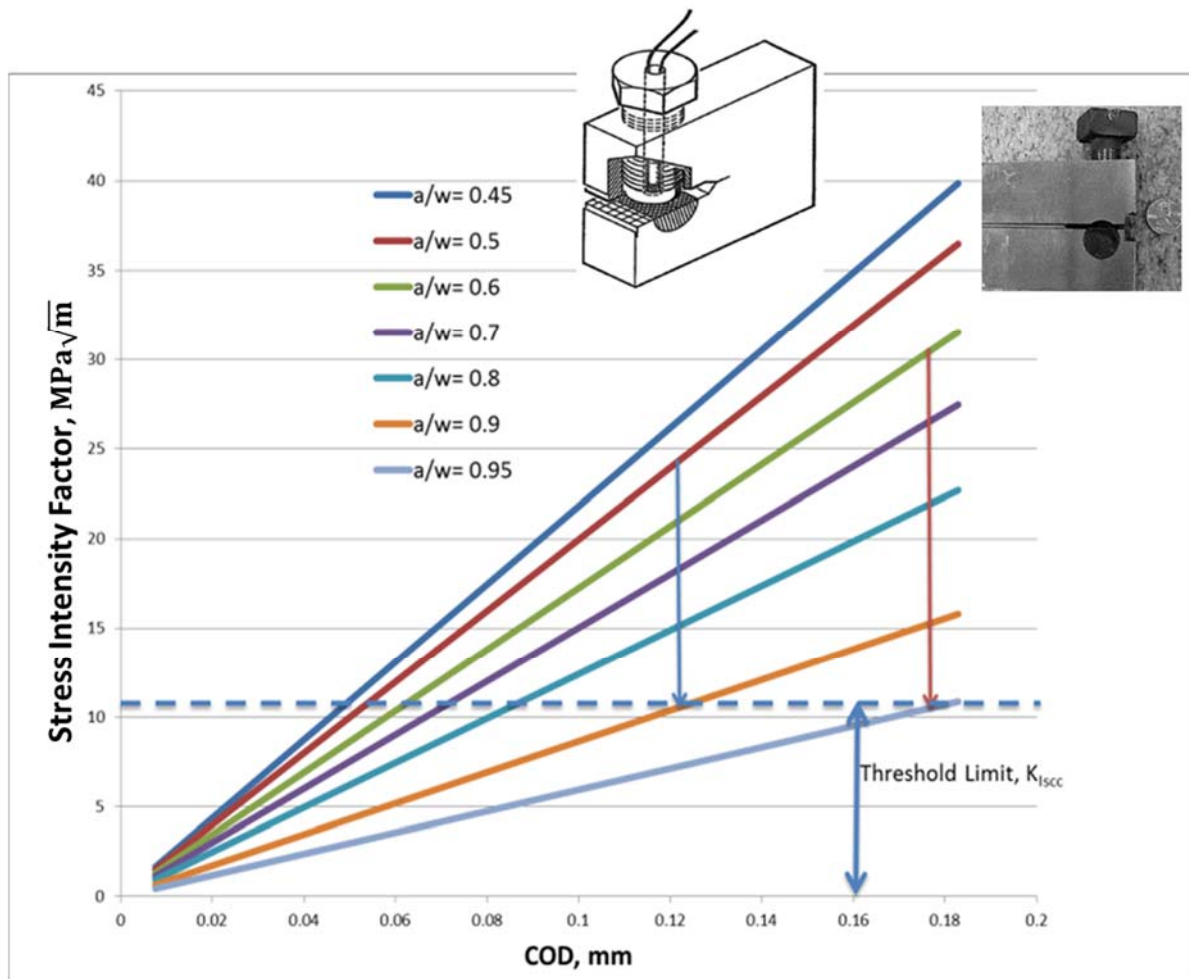


Figure 5. Expected crack growth behavior of “falling K ” constant displacement CT test

An instrumented bolt [28] with built-in load cell was selected for the bolt-load CT specimen. The design is shown in Figure 6. The feed-through on both the glass vessel (environmental cell) and the oven (see Sections 2.2 and 2.3) enabled a data acquisition system (DAS) to acquire load drop with time for a fixed displacement (COD). Figure 7 is a *typical* graph of load/temperature vs. time, which was obtained from the instrumented bolt-load CT test in Section 2.3. In Figure 7, the temperature record (green) was from a thermocouple, the “Baseline (37C)” data (yellow) were obtained from the instrumented bolt itself (threaded plug); and the “RT” (red) and the “37C” (blue) curves are the load vs. time data at room temperature and at 37 °C, respectively, for bolt-load CT specimens packed with dry salt in 75% RH environments (see test matrix in Table 3).

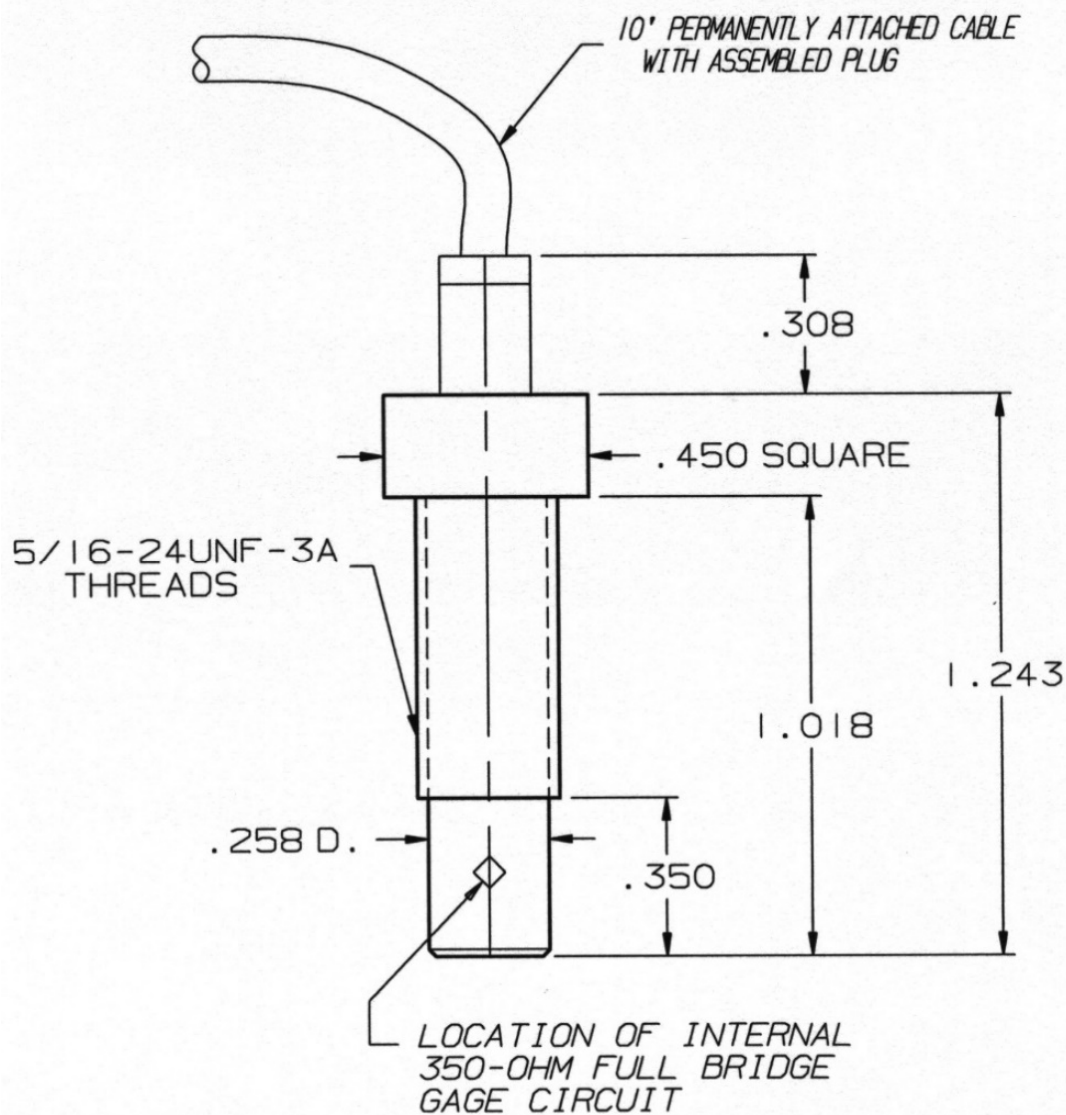


Figure 6. Instrumented bolt design

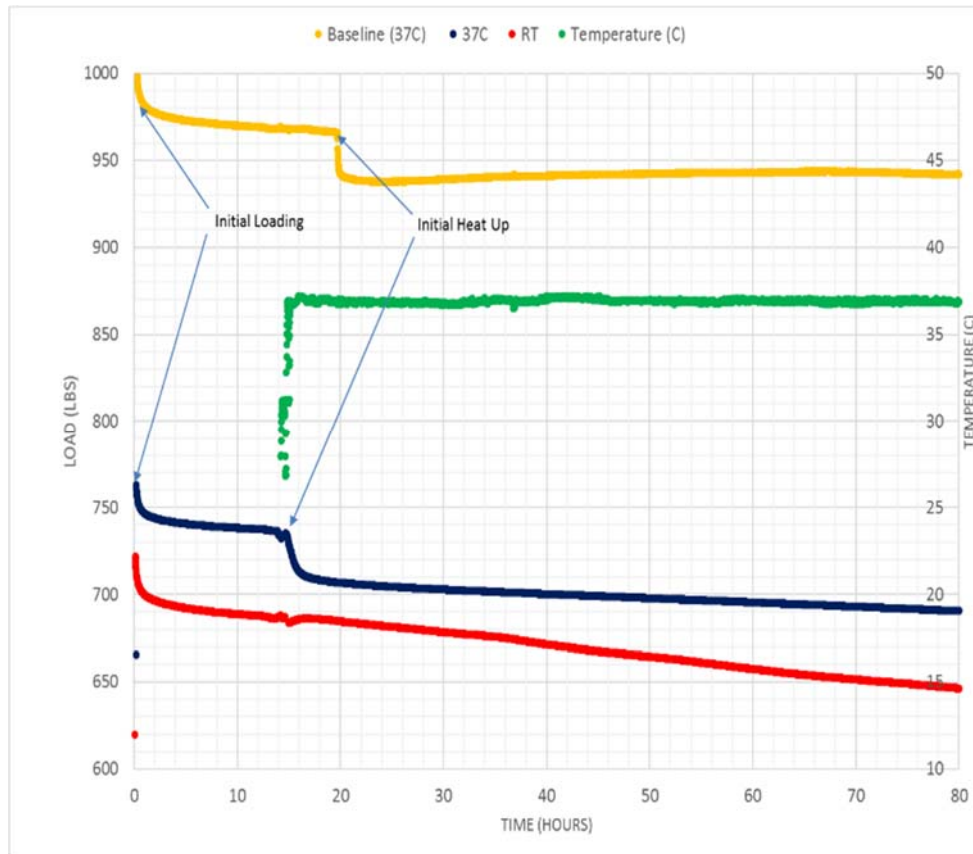


Figure 7. Typical load - time response of instrumented bolt

2.2 Crack Growth Rate Test with Mixture of Salt and Dust

Stress corrosion cracking may occur when chloride-bearing salts that may be present in a dust mixture deliquesce on the external surface of SNF canister in WRS regions. Experimental apparatus was designed to allow dried salt to deliquesce and the brine (electrolyte) to infuse naturally (via capillary action) to the crack front of the instrumented bolt-load CT specimens under temperature and humidity parameters relevant to the canister storage environmental conditions. The shakedown tests were conducted at 50 °C and over a range of relative humidity controlled by the guidance in ASTM E104, “*Standard Practice for Maintaining Constant Relative Humidity by Means of Aqueous Solutions.*” The salt assemblages used in the test were (1) mixture of artificial dust and deliquescent salts, and (2) a mixture of artificial dust and salt from dehydrated sea water (artificial sea salt).

2.2.1 Experiment

The bolt-load CT specimens were fabricated with 12.7 mm (½ in.) thick 304 stainless steel plate with 0.063 wt.% C archival heat from prior to 1980. Three conditions were tested and are summarized in Table 1. The dust/salt constituents are a mixture of CeO₂ + 2% mixture of

NaCl/KCl/CaCl₂ (Specimen 1) and a mixture of simulated inorganic dust and artificial sea salt (Specimens 2 and 3). The temperature and humidity conditions were selected to bound ambient conditions and were held constant at 50 °C. Constant relative humidity levels of 50% (Specimens 1 and 2) and 30% (Specimen 3) were maintained at all times for the duration of testing. The constant RH was achieved using ASTM E104, “*Standard Practice for Maintaining Constant Relative Humidity by Means of Aqueous Solutions.*” The artificial sea salt was prepared according to ASTM D1141, “*Standard Practice for the Preparation of Substitute Ocean Water.*” The salt/dust composition for Specimen 1 was chosen based on previous corrosion studies [29,30] as an artificially aggressive condition because of the high level of CaCl₂. The dust components, all non-water-soluble, provide a non-aggressive medium that distributes the salt components, that would undergo deliquescence to form a brine. The compositions for Specimens 2 & 3 were selected to be more relevant to service conditions of the canisters [31]. The schematic arrangement of the bolt-load CT in the constant humidity vessel (test cell) is illustrated in Figure 8.

Table 1..Experimental conditions of exposure in dry salt crack growth testing

Test Cell Number Specimen Number	Environmental Conditions	Simulated Dust
1	50 °C and 50% RH [†]	98% CeO ₂ [*] 0.8% NaCl 0.8% KCl 0.4% CaCl ₂
2	50 °C and 50% RH [†]	50% Washed Sand [*] (-200 mesh) ^{**} 12.5% Kaolin 12.5% Feldspar 25% Artificial Sea Salt [§]
3	50 °C and 30% RH [‡]	50% Washed Sand [*] (-200 mesh) ^{**} 12.5% Kaolin 12.5% Feldspar 25% Artificial Sea Salt [§]

* Secondary compounds of sea sand besides SiO₂ can be Zircon, Ilmenite and Rutile

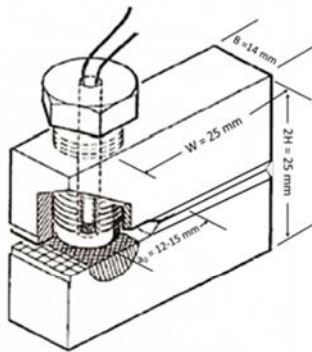
† Achieved using ASTM E104 saturated aqueous solution of NaBr

‡ Achieved using ASTM E104 saturated aqueous solution of MgCl₂

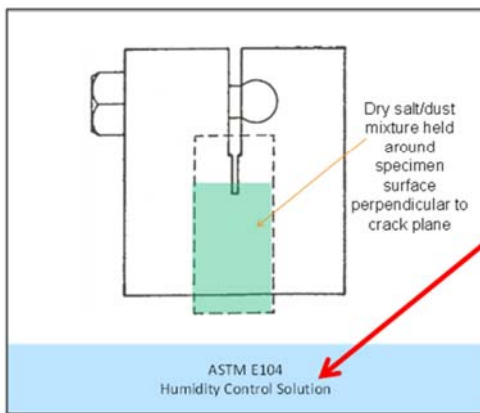
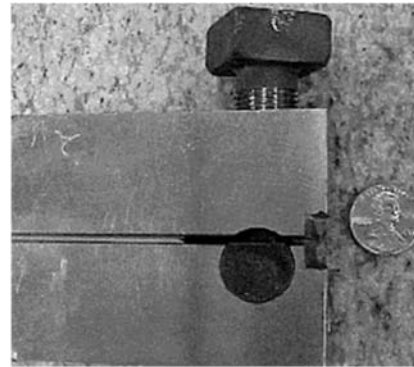
§ Composition and form as specified by ASTM D1141

* SRNL legacy salt/dust mixture – CeO₂ particle size is not available (surrogate for PuO₂)

** By standard conversion, the particle size for 200 mesh is 0.074 mm.



An Instrumented Bolt Measures the Load Drop With Crack Extension



Equilibrium Relative Humidity (ASTM E104):

Sodium Chloride

NaCl at 25 °C → 75 ± 0.6% RH

Sodium Bromide

NaBr at 50 °C → 50.9 ± 0.6% RH

Magnesium chloride

MgCl₂ at 50 °C → 30.5 ± 0.2% RH

Figure 8. Schematic arrangement of the bolt-load CT specimen in constant humidity vessel that is placed inside an oven with constant temperature

To gather visual evidence of the deliquescence and corrosion of the bolt-load CT specimens without unloading and removing from the test environment, 304L stainless steel teardrop coupons (Figure 9) were inserted in glass cradles next to the bolt-load CT specimens in each vessel (Figure 10). The dry salt was also packed between the teardrop specimen and its holder, and the crevice corrosion would not occur. The teardrop specimens were originally designed for another nuclear material surveillance program at SRNL. An autogenous weld was fabricated in the teardrop coupon to provide a similar weld microstructure as was present in those containers. All the specimens were exposed to the same experimental conditions for 5 months and then unloaded for analysis.

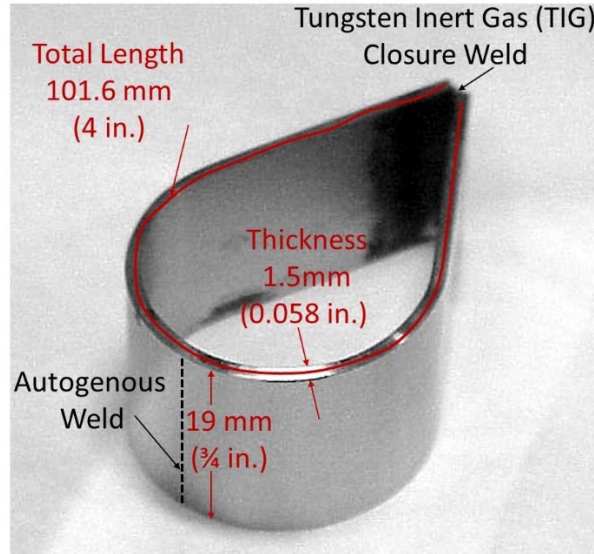


Figure 9. Teardrop coupon used to provide convenient assessment of the bolt-load CT specimen during CISCC test

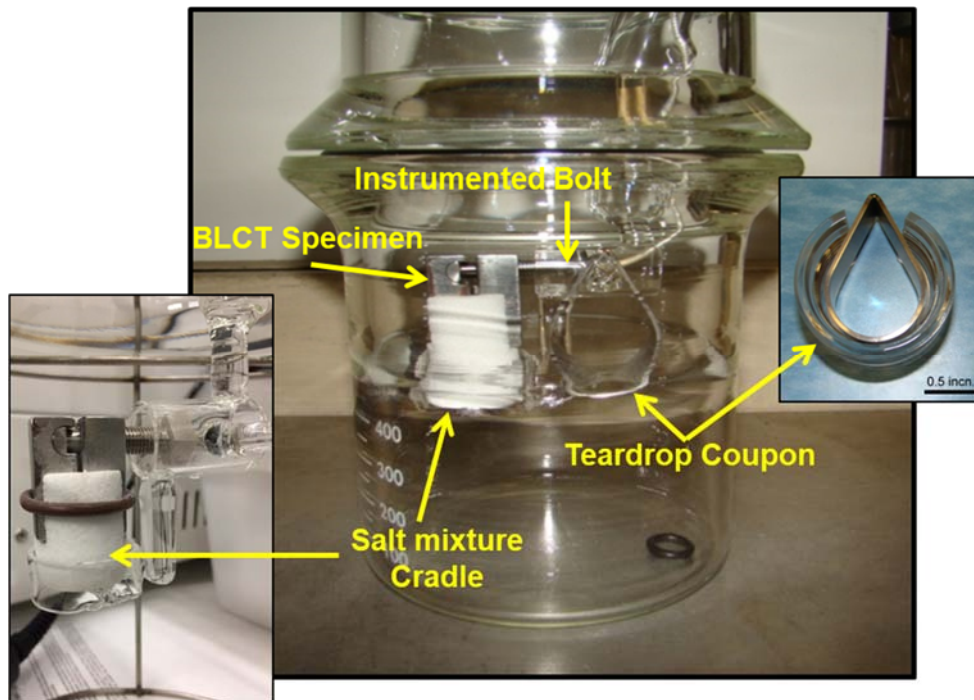


Figure 10. SCC test configuration showing the cradled instrumented bolt-load CT (BLCT) specimen and a companion teardrop coupon in a constant humidity vessel

As shown in Figure 11, three constant humidity vessels (test cells) with loaded specimens under conditions listed in Table 1 were placed inside an oven with temperature set to 50 °C. Note that absolute humidity of $\sim 30 \text{ g/m}^3$ is bounding in nature. At 50% RH and 50°C, the absolute humidity is 42 g/m^3 .



Figure 11. Experimental set up for CGR test using three different salt/dust mixtures and RH conditions at a constant oven temperature

2.2.2 Results

The specimens were removed after 5 months of exposure under the conditions in Table 1. Figure 12 shows the appearance of the specimens as they were removed from the test cells (constant humidity vessels) after exposure. Both the bolt-load CT and teardrop specimens in Cell 1 exhibited corrosion around where the specimens were in contact with dust/salt. They also had the dust/salt mixture clumped on their surfaces. The bolt-load CT and the teardrop specimens in Cells 2 and 3 (see Table 1) did not have any visible corrosion and only had a smaller amount of dust adherent to surfaces.

It appears that under the condition of 50 °C and 50% RH, the simulated dried salt residues deliquesce to provide adequate electrolyte which leads to pitting corrosion and cracking in 304 stainless steel, such as the bolt-load CT specimen in Cell 1. As shown in Figure 13, the cracking in this bolt-load CT specimen occurred in the side groove region and the nature of cracking was

not planar. Therefore, the associated stress intensity factor and the CGR were difficult to characterize. In the case of sea salt tests that used artificial sea salt/dust mixtures (Cells 2 and 3), the pitting corrosion or cracking was not present even when they were exposed to relative humidity that bounds possible service conditions. This is most likely due to the absence of a brine film in contact with the surface of the specimens. This observation suggests that capillary action to draw brine onto a crack face is not certain. That is, this one specimen shows that the occurrence of CISCC under deliquesce conditions with assumption that capillary forces would draw brine into a crack to wet a crack front is stochastic.



Figure 12. Specimens as removed from test cells (Cell 1: calcium-rich salt, Cell 2: sea salt)

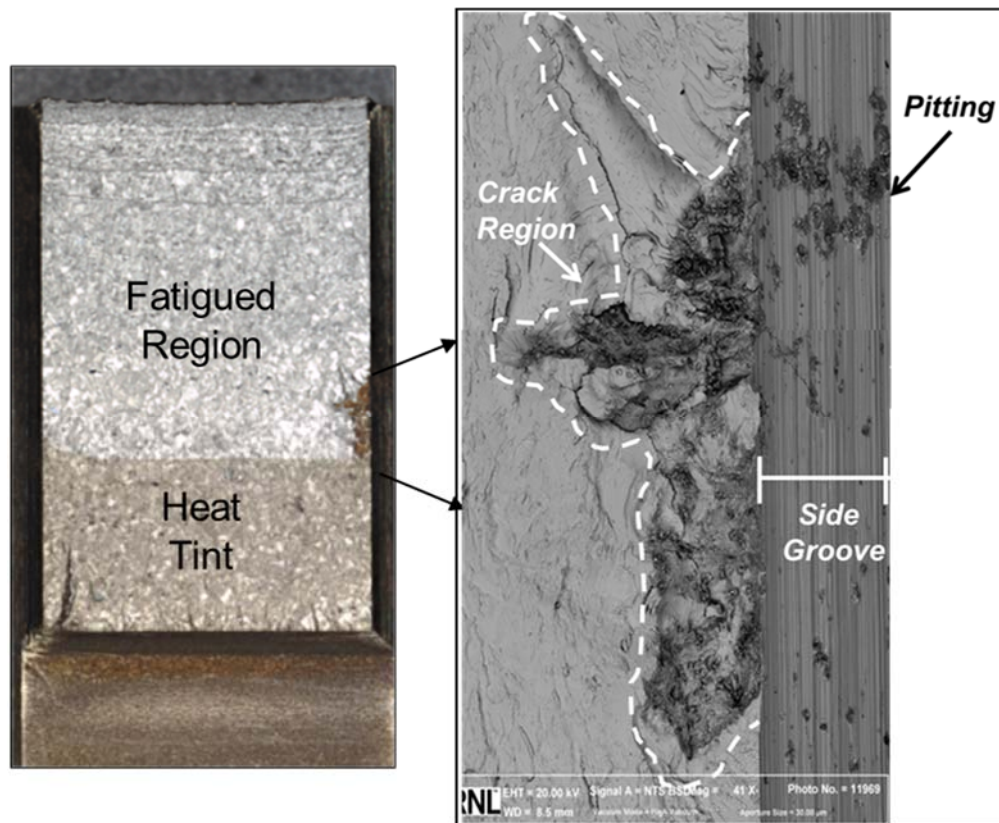


Figure 13. Optical and SEM images of the fracture surface of the bolt-load CT specimen (Specimen 1) exposed to simulated calcium-rich salt at 50 °C and 50% RH for 5 months

2.3 Crack Growth Rate Test with Dry Salt

This section describes the CGR testing with instrumented bolt-load CT specimens that were machined from two small plates from a mockup canister [15], which was constructed with dual-certified 304/304L stainless steel with 308L as the weld filler. The chemical compositions of the materials of construction are listed in Table 2 (balance is Fe). The experiments are similar to those reported in Section 2.2. The bolt-load CT was packed with dry salt (ASTM D1141 prepared and dried). Under favorable environmental conditions that occur in the test chamber, the brine from the naturally deliquescent salt is transported to the specimen crack front and may cause CISCC. The CGR is obtained from the elapsed time average of the difference between the initial and final crack lengths.

Table 2. Material Chemical Composition for Sandia mockup canister (wt.%) [15]

Materials	C	Co	Cr	Cu	Mn	Mo	N	Ni	P	S	Si
Base Metal 304/304L	0.0223	0.1865	18.1000	0.4225	1.7125	0.3180	0.0787	8.0270	0.0305	0.0023	0.2550
Weld Filler Lot 1 308L	0.014	—	19.66	0.16	1.70	0.11	0.058	9.56	0.025	0.010	0.39
Weld Filler Lot 2 308L	0.0012	—	19.71	0.192	1.730	0.071	0.053	9.750	0.024	0.012	0.368

2.3.1 Experiment

Figure 14 shows the two plates cut from a full-size mockup canister [15]. One of the plates contains an axial (longitudinal) weld and the other has a circumferential (girth) weld. Figure 14 also shows the three bolt-load CT specimens machined from each plate - one in the base metal and two in the HAZ. Note that the mockup canister wall thickness is 16 mm ($\frac{5}{8}$ in.). Therefore, the thickness of the flat bolt-load CT specimens as machined from the curved plate would be reduced but still satisfies ASTM E1681 requirement (Figure 4).

These bolt-load CT specimens were designed such that the intended crack growth direction is identical in all specimens, that is, all the expected crack extensions are parallel to the rolling direction of the plate (i.e., T-L, the weakest direction for the crack to propagate mechanically in this plate, where K_{IC} value is the lowest). During the canister fabrication, the plate is cold formed into cylindrical shape as a section of the canister, then all the sections are joined by submerged arc welding (SAW). As schematically indicated in Fig. 14, the loading experienced by the bolt-load CT is “Bolt Load + RS3” or “Bolt-Load+RS4,” where the “bolt load” is the tensile stress exerted by tightening the instrumented bolt; RS3 represents the WRS perpendicular to the circumferential weld; and RS4 is the WRS parallel to the axial weld. Note that RS3 and RS4 have been obtained experimentally [15] and numerically by finite element simulation [32] (see Fig. 15).

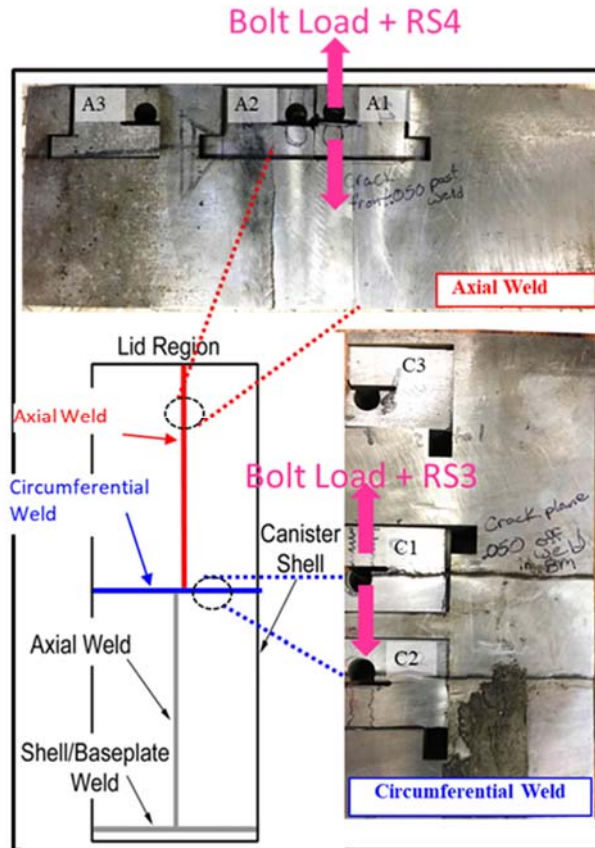


Figure 14. The Bolt-Load CT specimens as machined from two plates cut from the mockup canister

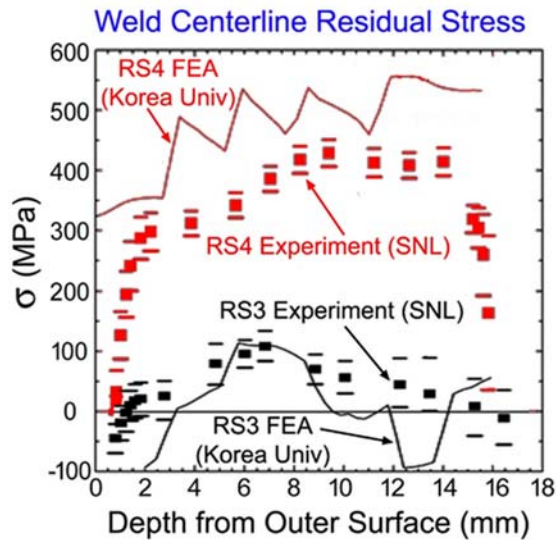


Figure 15. The WRS Components RS3 (Perpendicular to Circumferential Weld) and RS4 (Parallel to the Axial Weld) [15,32] (Courtesy of Korea University under I-NERI/USA-ROK)

The design and the pre-cracking procedure of the bolt-load CT specimens used in this experiment have been described in Section 2.1 (ASME E1681). Figure 16 shows that the dry salt used to induce CISCC was packed around the notch region of the bolt-load CT specimen. The dry salt was obtained from dehydrated artificial sea water prepared according to ASTM D1141, “*Standard Practice for the Preparation of Substitute Ocean Water.*” A chemical-free cellulose wick (Figure 17) [33] can be seen to be inserted at the end of the machined notch of the bolt-load CT specimen (see Figure 16 (a)) to ensure that the brine from the deliquescing salt is transported evenly to the crack front.

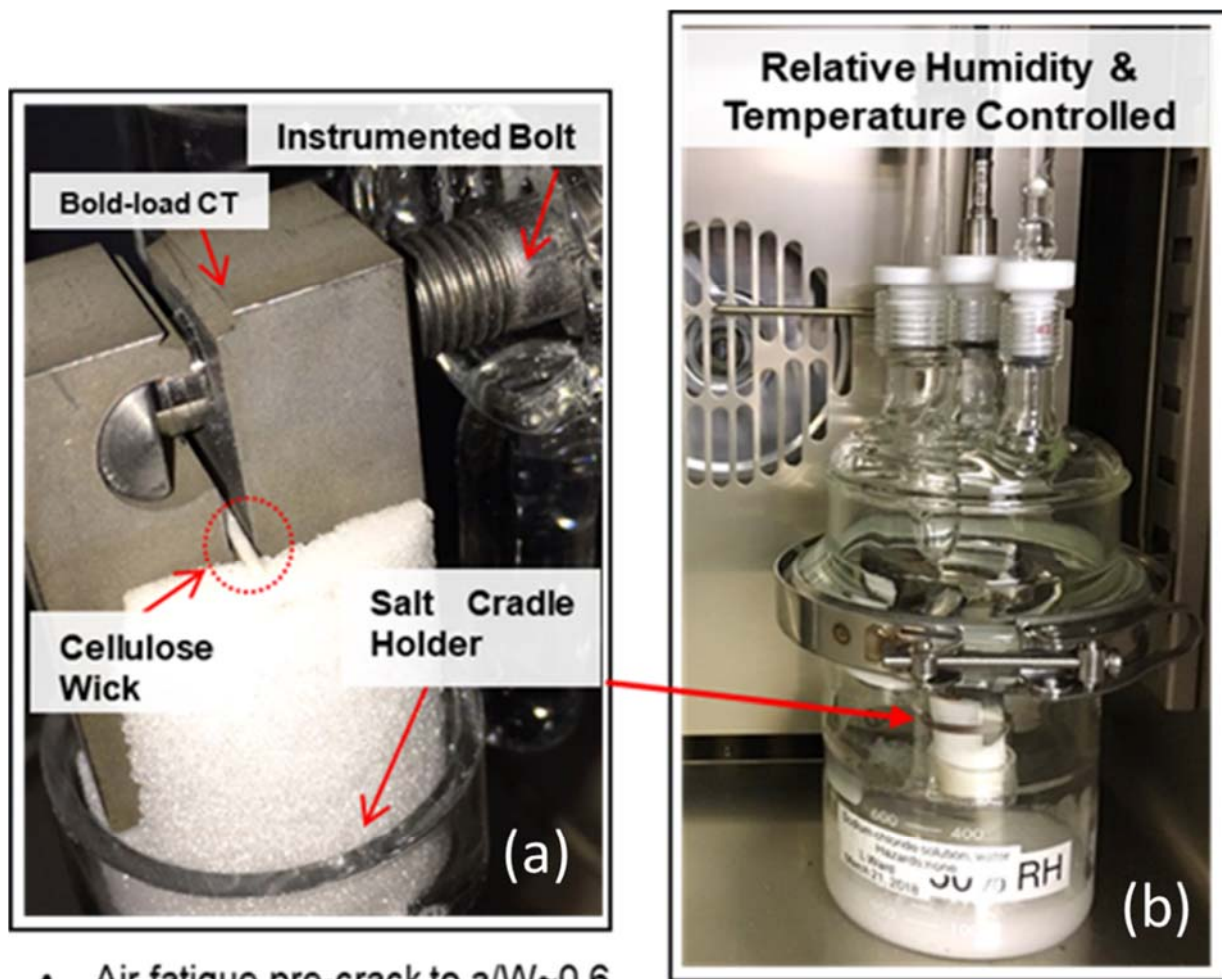


Figure 16. Typical configuration of the bolt-load CT specimen packed with dry salt (a) and then installed in a closed glass vessel with teardrop coupon under constant humidity condition (b)



Figure 17. Cellulose wicks (in vendor package and in a test tray with water drops) used to transport deliquescing salt to crack front in bolt-load CT specimens

The dry salt-packed bolt-load CT specimen was then installed inside a closed glass vessel, as seen in Figure 16 (b). The desired 75% RH at room temperature and at 37 °C can be achieved with ASTM E104, “*Standard Practice for Maintaining Constant Relative Humidity by Means of Aqueous Solutions*” by using sodium chloride (NaCl) aqueous saturated salt solution in the bottom of the glass vessel (Figure 16 (b)). Table 3 is the test matrix for the bolt-load CT specimens in this experiment.

Table 3. Crack growth rate test matrix using bolt-load CT specimens

Sample	Sample ID	Temperature	RH	Thermal History	Orientation
Axial 1	A1	22 °C (Room Temperature)	75%	HAZ	TL
Circ. 2	C2			HAZ	
Axial 3	A3			BM	
Axial 2	A2	37 °C	75%	HAZ	TL
Circ. 1	C1			HAZ	
Circ. 3	C3			BM	

- Samples 1 & 2 cut from heat affected zone (HAZ)
- Sample 3 cut from Base Metal of plate (BM)
- Dehydrated Salt Residues (95 °C for 72 hrs) from ASTM D1141 simulated sea salt

2.3.2 Results

The base metal bolt-load CT specimens, A3 and C3, (see Fig. 14 and Table 3) were removed from the test apparatus at the end of two months; while specimens A1, A2, C1, and C2, which are associated with the HAZ, remained in the test setup for six months. All specimens after testing were cleaned by following ASTM G1, “*Standard Practice for Preparing, Cleaning, and Evaluating Corrosion Test Specimens.*” Final crack lengths were established first by heat tinting the specimens at 350°C for 30 minutes to mark the final crack front, then break open the specimen in halves by fatigue. The crack lengths were measured with an optical microscope in compliance with ASTM E1681 at the transition from heat tint and un-oxidized fatigue surface. Figure 18 is a typical fractured surface (from Specimen C1 after exposure for six months). It shows the regions of fatigue pre-cracking, CISCC (Δa), and the final fracture by fatigue.

Table 4 summarizes the CISCC test results for all six bolt-load CT specimens up to six-month exposure. It is noticed that higher test temperature would not always cause more crack growth (Δa) within the temperature range in this test (i.e., Specimen C1 at 37 °C vs. C2 at room temperature or 24 ±2 °C). It is also likely that these measurements were within the experimental error band. Nevertheless, it is obvious that the crack growth near the axial weld (Specimens A1 and A2) was faster than that in the circumferential weld (Specimens C2 and C1). Note that the initial mechanical load through the bolt was similar in all specimens (~33 MPa√m), but the residual stress (RS4) acting on Specimens A1 and A2 was indeed much higher than RS3 on Specimens C1 and C2, as suggested by Figure 15 (assuming that the original WRS was not altered significantly by plate cutting and by specimen fabrication using EDM). Therefore, the effective loading (WRS plus mechanical applied load) on Specimens A1 and A2 was higher than that on C1 and C2. This fact may be used to explain why A1 and A2 have greater crack growths (Δa) than C1 and C2, regardless of the test temperatures.

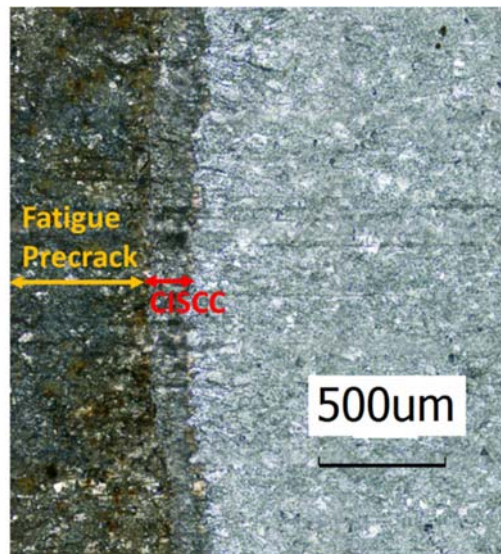


Figure 18. Typical fracture surface under CISCC (from Specimen C1 in 75% RH at 37 °C for 6 months)

Table 4. Results of bolt-load CT tests up to six months

304/304L Specimen	Actual Temp. (°C)	Actual RH (%)	Initial <i>a/w</i>	Final <i>a/w</i>	Initial <i>K</i> (MPa√m)	Δa (μm)
C1 (HAZ)	37	74±3	0.60 ^b	0.62 ^b	32.4	137 ^b
C2 (HAZ)	24±2	74±3	0.50 ^c	0.52 ^b	34.6	230 ^b
C3 (BM) (2-month exp.)	37	74±3	0.78	0.78 ^b	33.7	-
A1 (HAZ)	24±2	74±3	0.63 ^b	0.65 ^b	33.1	526 ^b
A2 (HAZ)	37	74±3	0.60 ^{ac}	0.62 ^b	34.0	614 ^c
A3 (BM) (2-month exp.)	24±2	74±3	0.61 ^b	0.62 ^b	33.1	188 ^b

a: Initial values measured from side groove crack growth measurements

b: Measured using optical average of crack fronts from fracture surface

c: Estimated from specimen compliance

The crack growth rates determined from the bolt-load CT specimens after 2- and 6-month exposure at room temperature and 37 °C are the test time average of the total crack growths (Δa) from Table 4. These new data points, circled within the two ellipses (in cyan) in Figure 19, are added to the historical database for stainless steels under CISC environments [16-19]. Also included in Figure 19 are recent results from Korea University [21,22], through the DOE I-NERI project [20], where immersion tests were carried out for 304 stainless steel standard CT specimens in 5% salinity solution at 50 °C (see Section 2.4). It appears that all CGR data can be represented by a straight regression line in semi-logarithmic scale [2] in Figure 19:

$$\log(\dot{a}) = 3.8444 - 4444.444 \left(\frac{1}{T}\right) \quad (2)$$

where \dot{a} is the CGR in m/s and T is the test temperature in kelvin.

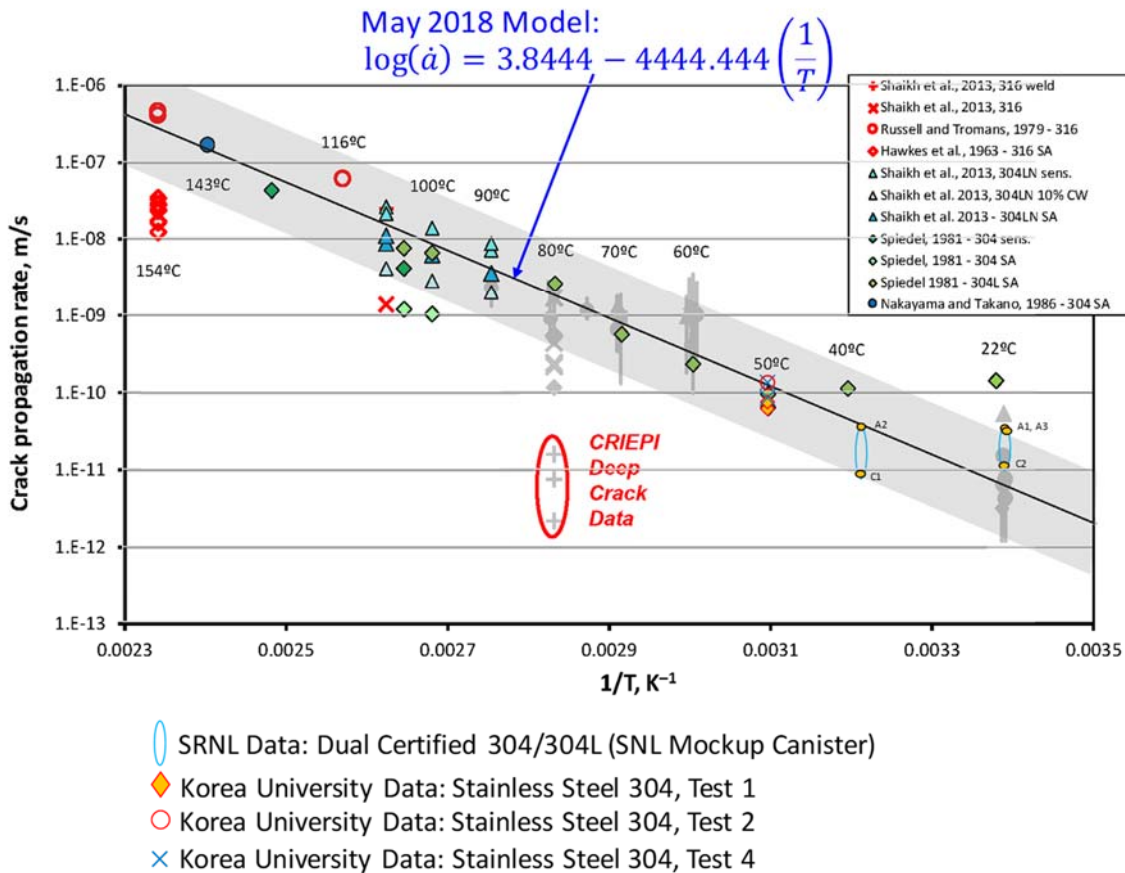


Figure 19. Chloride-induced stress corrosion crack growth rates under wide range of exposure conditions (original figure courtesy of Sandia National Laboratories [17-19])

2.4 I-NERI: Korea University Compact Tension Test for CISCC

The Korea University has been developing CGR tests in CISCC conditions as part of the research scope under I-NERI/USA-ROK Project Number 2016-001-K: “Flaw Stability and Stress Corrosion Cracking of Austenitic Stainless Steel Canisters for Long Term Storage and Transportation of LWR Used Fuel” [20]. The CGR data are used to support the development of ASME BPVC Section XI Code Case N-860, entitled “Examination Requirements and Acceptance Standards for Spent Nuclear Fuel Storage and Transportation Containment Systems.”

2.4.1 Experiment

A new experimental apparatus has been designed for CGR test under CISCC conditions using standard CT specimen. As seen in Figure 20, the bolt on top of the apparatus can be tightened to provide constant displacement to the CT specimen, and the connected load cell measures the load as a function of time. To expose the crack tip to CISCC environment directly, specimen is immersed into a chloride solution and a cap made of polymer is put on a glass chamber to prevent

evaporation. Jigs are made to suppress the bending and rotation due to loading throughout the test. The components of the apparatus were all made from 304 stainless steel, which is the same as the material to be tested. The chemical composition of 304 stainless steel used at KU is listed in Table 5.

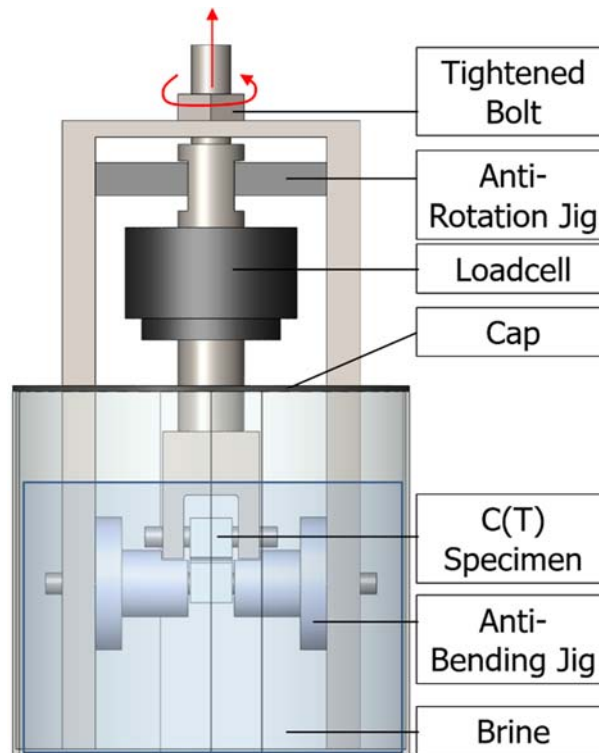


**Figure 20. Schematic diagram of the CGR test apparatus with standard CT specimen
(Courtesy of Korea University under I-NERI/USA-ROK)**

Table 5. Chemical compositions of 304 stainless steel (wt.%) – Korea University

C	Si	Mn	P	S	Ni	Cr
0.05	0.62	1.01	0.029	0.004	8.07	18.22

The standard CT specimens were fabricated according to ASTM E1820, “*Standard Test Method for Measurement of Fracture Toughness.*” The specimen design is shown in Fig. 21, where W is 25.4 mm and thickness B is 12.7 mm (i.e., $\frac{1}{2}T$ compact tension specimen). The specimens were fatigue pre-cracked with MTS 810 servo hydraulic material testing system, then tinted at 400 °C to distinguish any crack growth due to CISCC.

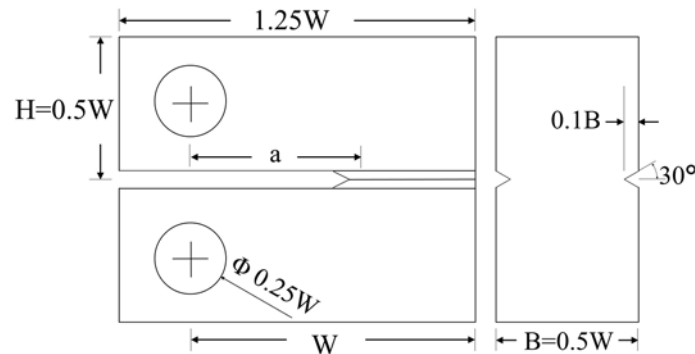


Figure 21. Standard compact tension specimen as recommended by ASTM E1820 (Courtesy of Korea University under I-NERI/USA-ROK)

The CT specimen was mounted in the apparatus (Figure 20) and immersed in a chloride solution with 5 % salinity composed of artificial sea salt. This is considered as conservative because the average salinity of seawater is 3 %. Efforts were made to minimize evaporation. Multiple sets of the apparatus with CT specimen installed were placed inside an environmental control chamber, which was maintained at 50 °C and 95 % RH (see Figure 22). The strain gages in the apparatus were calibrated to compensate the temperature change in the environmental chamber. The bolt was tightened according to the desired loading on the CT specimen. Note that this is a constant displacement test, therefore, the load decreases gradually as CISCC occurs, which is similar to the load vs. time relationship presented in Figure 7 (for SRNL test).



Figure 22. Korea University CISCC test conducted in an environmental control chamber (Courtesy of Korea University under I-NERI/USA-ROK)

2.4.2 Results

After the experiment was completed, the CT specimen was broken in halves to reveal the fracture surface. A typical fracture surface obtained by KU is shown in Figure 23 and the SCC can be identified under a microscope. The initial crack length (pre-cracked length) can be measured on the fracture surface by using the 9-point average method as recommended in ASTM E1820. The stress intensity factors are also calculated with ASTM E1820 formulation.

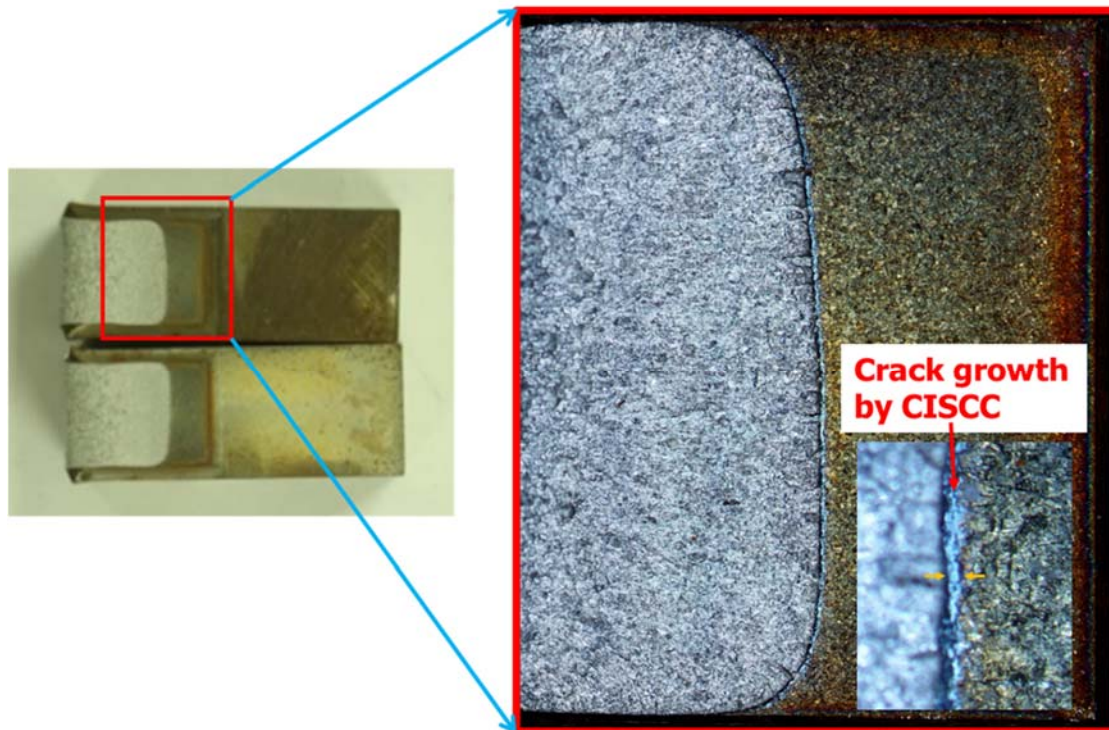


Figure 23. Typical fracture surface of CT specimen at KU with SCC indicated by arrows in the inset (Courtesy of Korea University under I-NERI/USA-ROK)

Four sets of the CISCC test with a total of 11 specimens have been completed [21,22]. The results are summarized in Table 6. The CGR for each specimen was also plotted in Figure 19. As discussed in Section 2.3.2, the data trend is consistent with other stainless steel test results reported in the literature, which were independently obtained from various laboratories with different exposure conditions. It can be seen that the chloride induced CGR appears to be strongly dependent on temperature.

Table 6. . Summary of CISCC test results from Korea University [21,22] (304 stainless steel immersed in a chloride solution with 5 % salinity at 50 °C)

Test	Specimen	Experimental periods [s]	Crack growth length [mm]	Average crack growth rate [m/s]	Initial stress intensity factor [MPa·√m]	Final stress intensity factor [MPa·√m]	Pin material
1	1	2,417,472	0.141	5.8E-11	49.2	45.1	SS304
	2		0.204	7.3E-11	51.7	46.2	
2	1	1,225,908	0.163	1.3E-10	74.3	53.2	SS304
	2		0.101	8.2E-11	65.7	49.5	
3	1	6,291,315	0	0	27.5	20.7	SS304
	2		0	0	20.7	15.3	
	3		0	0	30.7	23.2	
4	1	3,467,160	0	0	17.1	15.1	SS304 with Cr plating
	2		0	0	19.5	16.0	
	3		0.466	1.3E-10	40.7	38.7	
	4		0.451	1.3E-10	21.3	17.2	

(Courtesy of Korea University under I-NERI/USA-ROK)

The CGR results in Table 6 are plotted in Figure 24 as a function of stress intensity factor (K). Along with other related test data obtained from CRIEPI, it seems to indicate that the CGR under CISCC conditions is insensitive to stress intensity factor (i.e., crack tip loading).

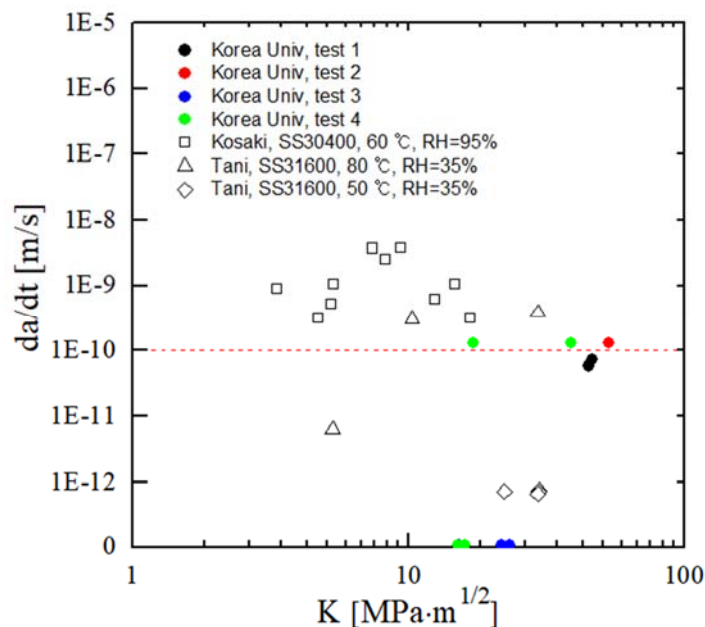


Figure 24. Dependence of crack growth rate (da/dt) on stress intensity factor (K) (Courtesy of Korea University under I-NERI/USA-ROK)

3. COMPANION TEARDROP SPECIMENS

The teardrop specimens were fabricated by bending a rectangular 304 stainless steel strip of $19.1 \times 101.6 \times 0.165$ mm ($0.75 \times 4 \times 0.065$ in.) around a 25.4 mm (1 in.) mandrel and then joining the ends by tungsten inert gas (TIG) welding. The teardrop coupon has a transverse autogenous weld at the center of curvature (apex) in the rounded section (see Figure 9), which was originally designed to simulate the weld microstructure in the weld region of a DOE storage container (e.g., [30,34]), and has been used as surveillance coupon for corrosion tests. Finite element analysis was conducted (Figure 25) [29,30] to reveal the high stress region resulting from the fabrication process in order to provide insight for SCC initiation. These teardrop coupons were adopted for the current investigation of CISCC in SNF canisters as a convenient indicator to provide a rapid assessment for the susceptibility of cracking and pitting. They were used as the companion samples with the instrumented bolt-load CT for the determination of CGR (Sections 2.2 and 2.3).

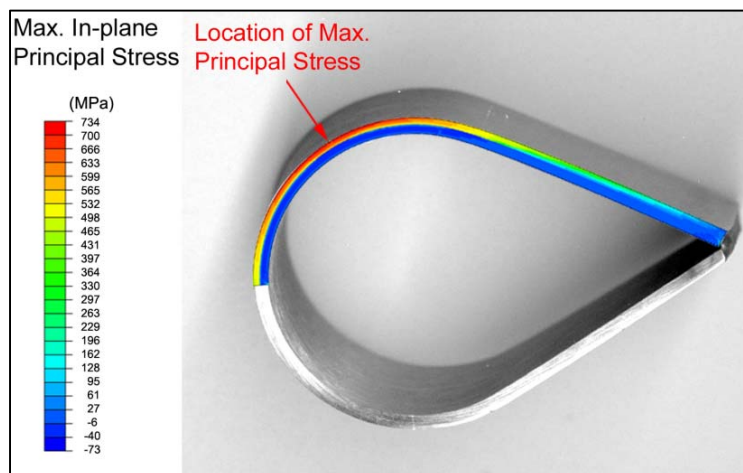


Figure 25. The location of maximum stress in the tear drop specimen [29,30]

3.1 Experimental Observation and Characterization

This section reports the detailed metallographic examination and analysis of the teardrop coupon, which was held in a glass cradle containing high level of CaCl_2 (0.4%) at 50 °C and 50% RH for 5 months (Test Cell No. 1 in Table 1). The exposed teardrop coupon (Sample 1) exhibited a region of adherent dust in the location where the salt/dust assemblage contacted the sample, as shown in Figure 26 (a). To remove the dust, the sample was cleaned in de-ionized water followed with an isopropanol rinse. After cleaning and drying, significant corrosion was observed as in Figure 26 (b). It was estimated that this area is about $0.25\text{-}0.28$ cm² (0.58 cm from top to bottom and 0.61 cm from left to right), on which about 6% of the area contained pits.

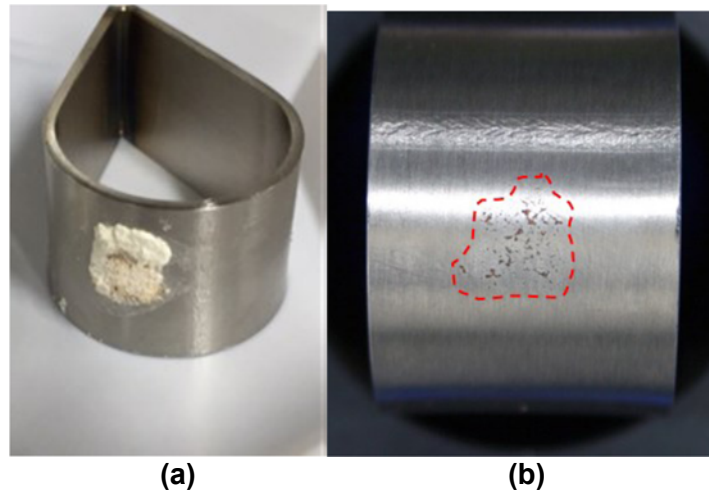


Figure 26. Adherent dust on teardrop Sample No. 1 following test (a) and the post-cleaning image with outlined corrosion region (b)

This teardrop coupon was subject to additional characterization and imaging [18.4] to further investigate pitting and cracking. The corroded region (Figure 26 (b)) was imaged using a laser confocal microscope (LCM) to identify the areas of interest (Figure 27). In particular, the LCM images of Area A and Area B in Figures 28 and 29 provide the depth information of the corrosion (pitted) area. Area 1 was sectioned along Lines A and B to show their linear profiles in the thickness direction (Figure 28).

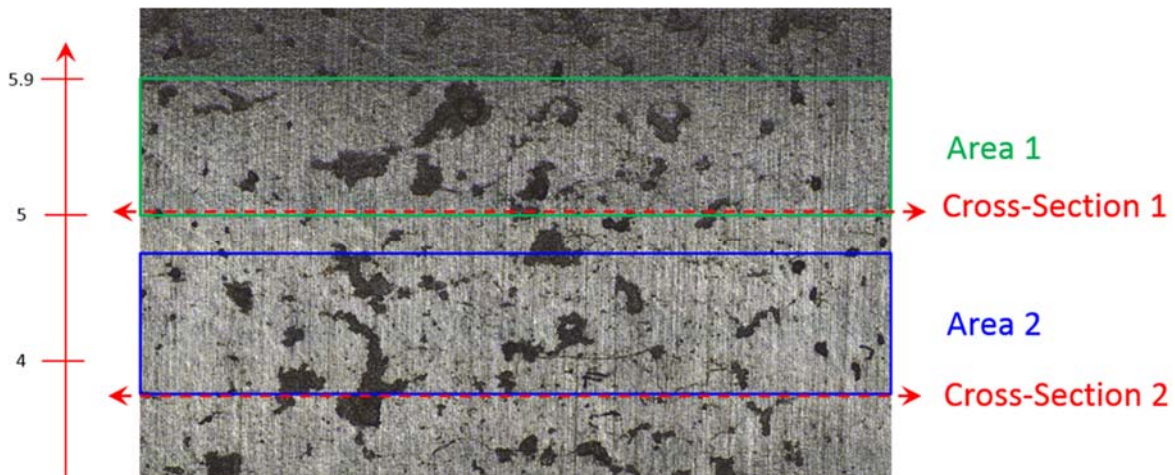


Figure 27. Image of the corrosion region on Sample 1

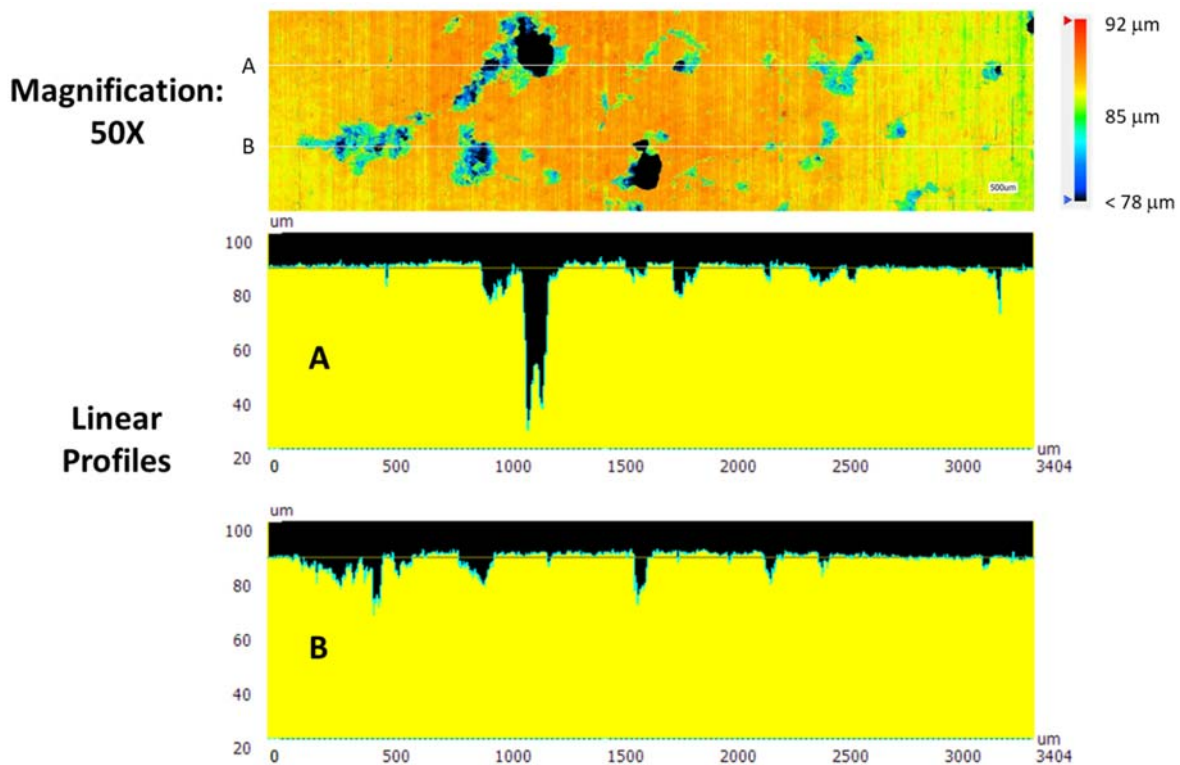


Figure 28. The LCM images of Area 1 in the corrosion area and the linear profiles of the cross-sections along Lines A and B, respectively

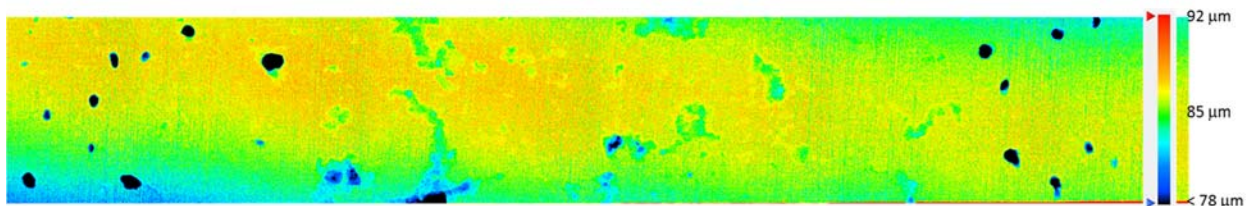


Figure 29. The LCM images of Area 2 in the corrosion area

Cross-section B from Area 1 was mounted, polished, and electrolytically etched with oxalic acid (10%). The cross section was then imaged at 50X to observe cracking morphology. Figure 30 shows the interaction of cracks and grains. Based on these images, cracking appears primarily transgranular. The depth of the left crack in Figure 30 is about $200\mu\text{m}$, corresponds to an average crack growth rate of 0.48 mm/year based on the exposure time of 5 months. Similarly, metallography analysis was also performed in Area 2 and its cross-section. The pits and SCC can be seen in Figure 31. Figures 30 and 31 demonstrate that the cracks below the teardrop coupon surface are interconnected. In addition, the smallest pits, in terms of diameter and pit depth, would develop networks of “long” cracks below the surface.

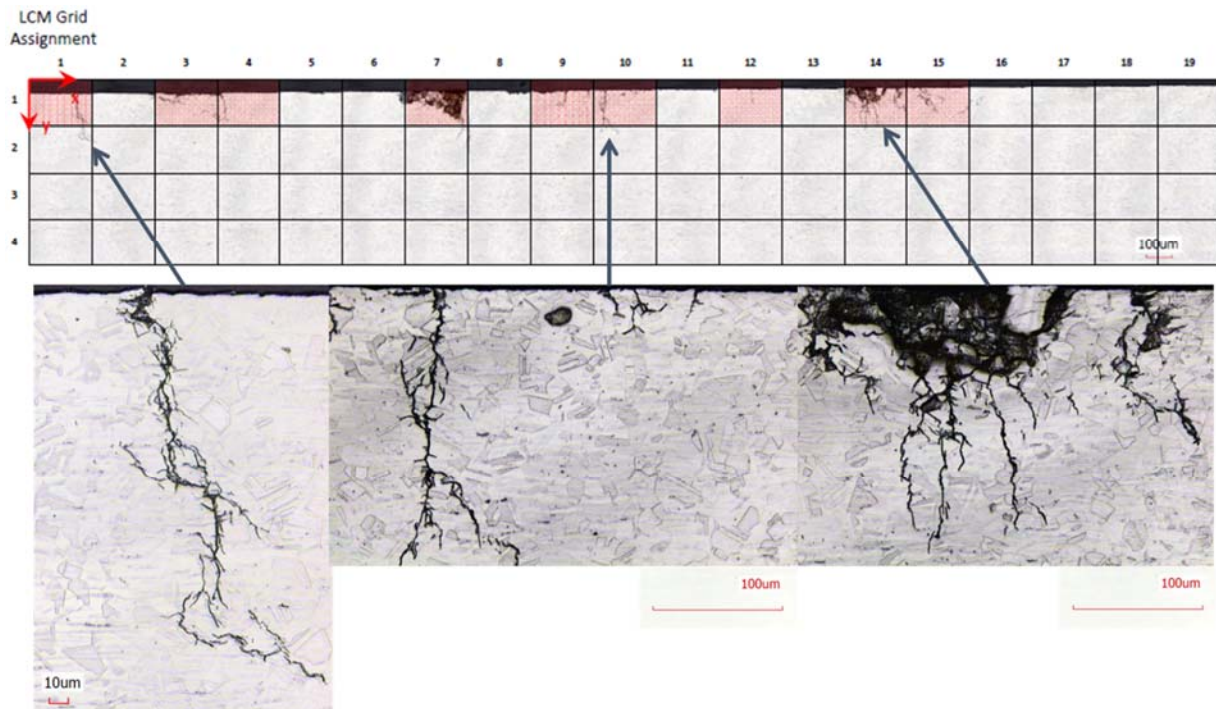


Figure 30. Images of cross-section B in Area 1 show transgranular stress corrosion cracks and pitting corrosion

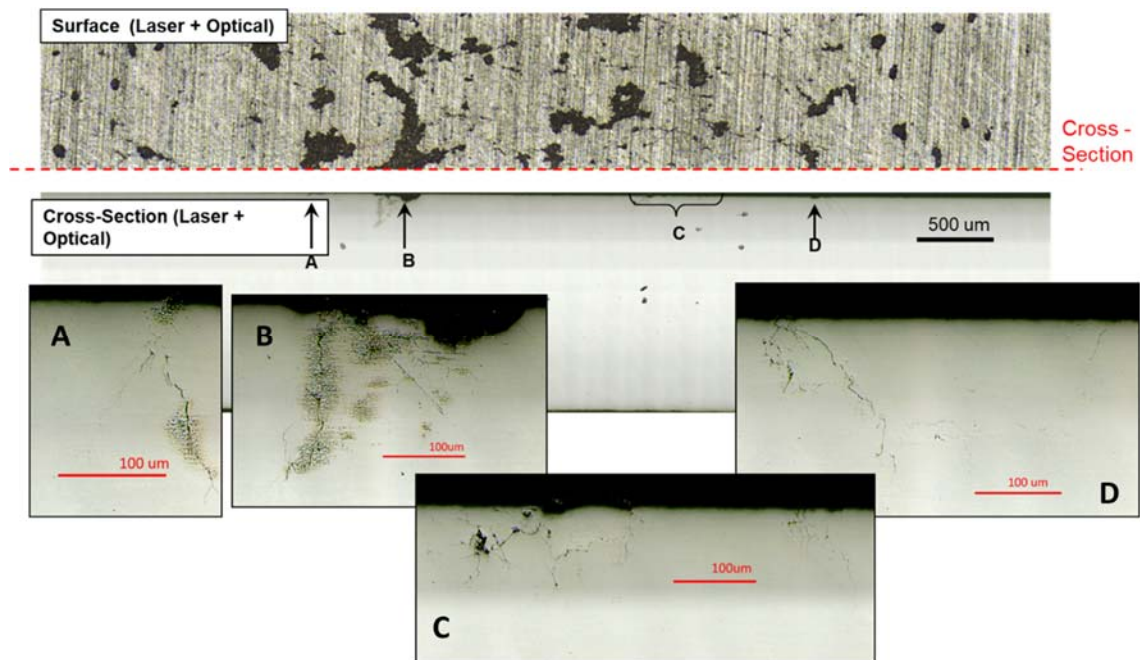


Figure 31. Images of the cross-section in Area 2 show transgranular stress corrosion cracks and pitting corrosion

Additional characterization of regions A, B, C, and D in the cross-section of Area 2 (Figure 31) were conducted. The pit depths and the associate SCC depth (lengths) were measured and indicated in Figures 32.

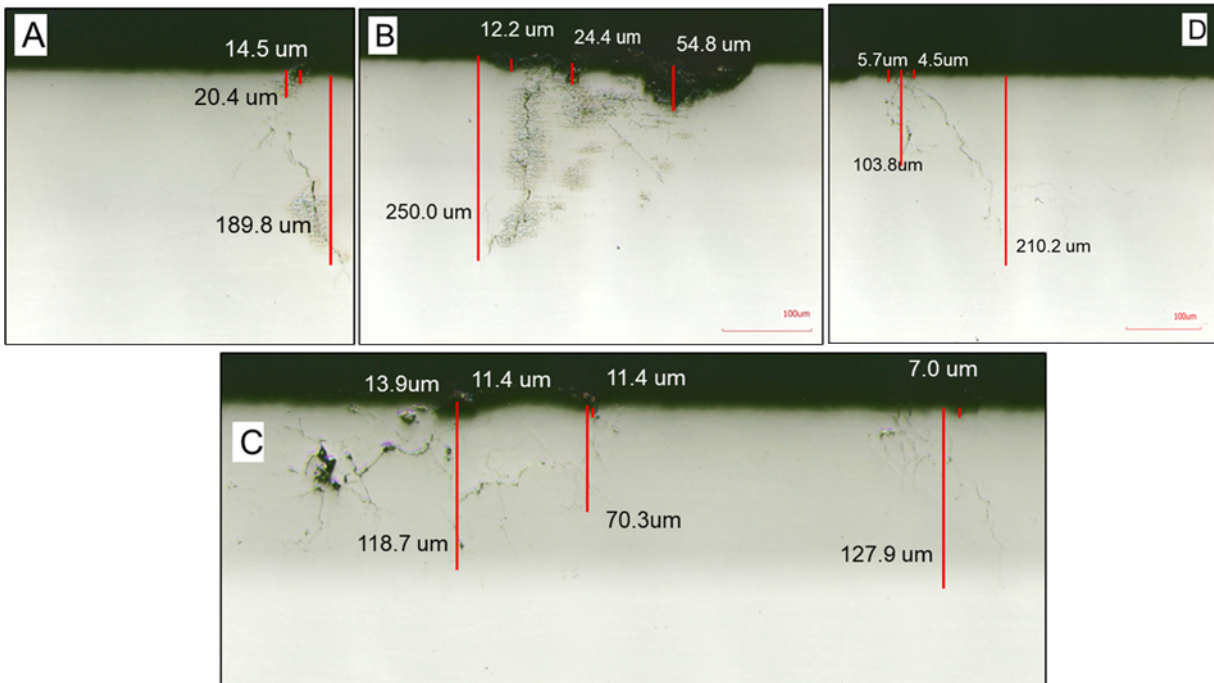


Figure 32. Characterization of pits and the associated stress corrosion cracks in sectioned teardrop coupon Sample 1

The one-to-one correspondence of pit depth and its associated crack depth (length) from Figure 32 is plotted in Figure 33 with symbol \blacklozenge . The CGR for each SCC was obtained by averaging the crack depth with respect to the duration of the test (5 months). The result is also plotted in Figure 33 and marked by \times . This result indicates that the crack depth in teardrop specimens is not necessarily related to pit depth [23].

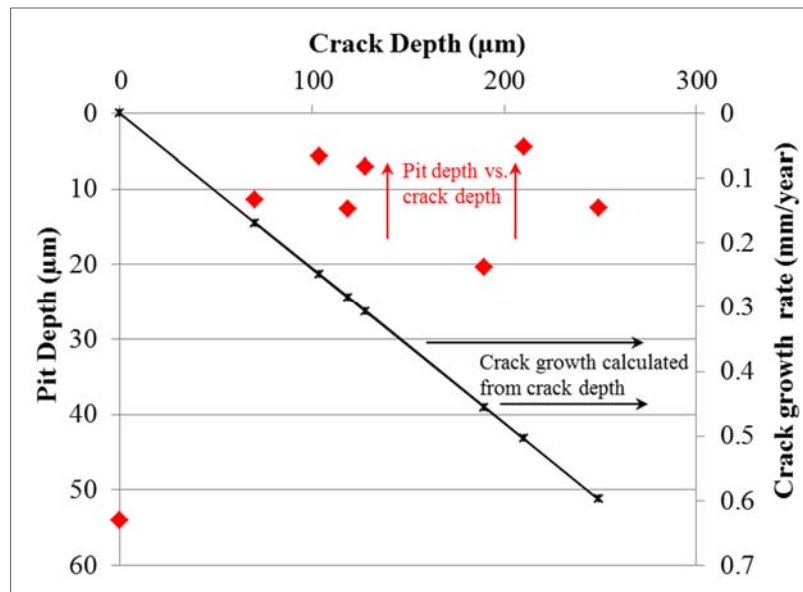


Figure 33. Relationship between pit depth and the associated crack depth (symbol ♦) as well as the corresponding crack growth rate (symbol ×) as converted from crack depth averaged by test duration (5 months)

3.2 Additional Artificial Sea Salt Testing

In the test described in Section 2.2, Test Cell Numbers 2 and 3 (see Table 1) used dust mixtures with 25% artificial sea salt. No crack growth in the bolt-load CT specimens was observed and no corrosion (pitting) was present on the companion teardrop coupons after exposure for 5 months [12,13,23]. This seems to imply that an environment conducive to crack growth may not exist.

Follow-up tests were conducted with sea salt at 50 °C and 50% RH using teardrop coupons. Results indicated that an aggressive nature of the environment was indeed established, that is, the teardrop specimens did crack after 3 months under these conditions. Figure 34 shows results from these tests and illustrates the presence of CISCC in the teardrop coupons. Specimens are shown in Figure 34 (a), (b), and (c) for 100% sea salt, 25% sea salt/75% CeO₂, and 25% sea salt/75% artificial dust conditions, respectively.

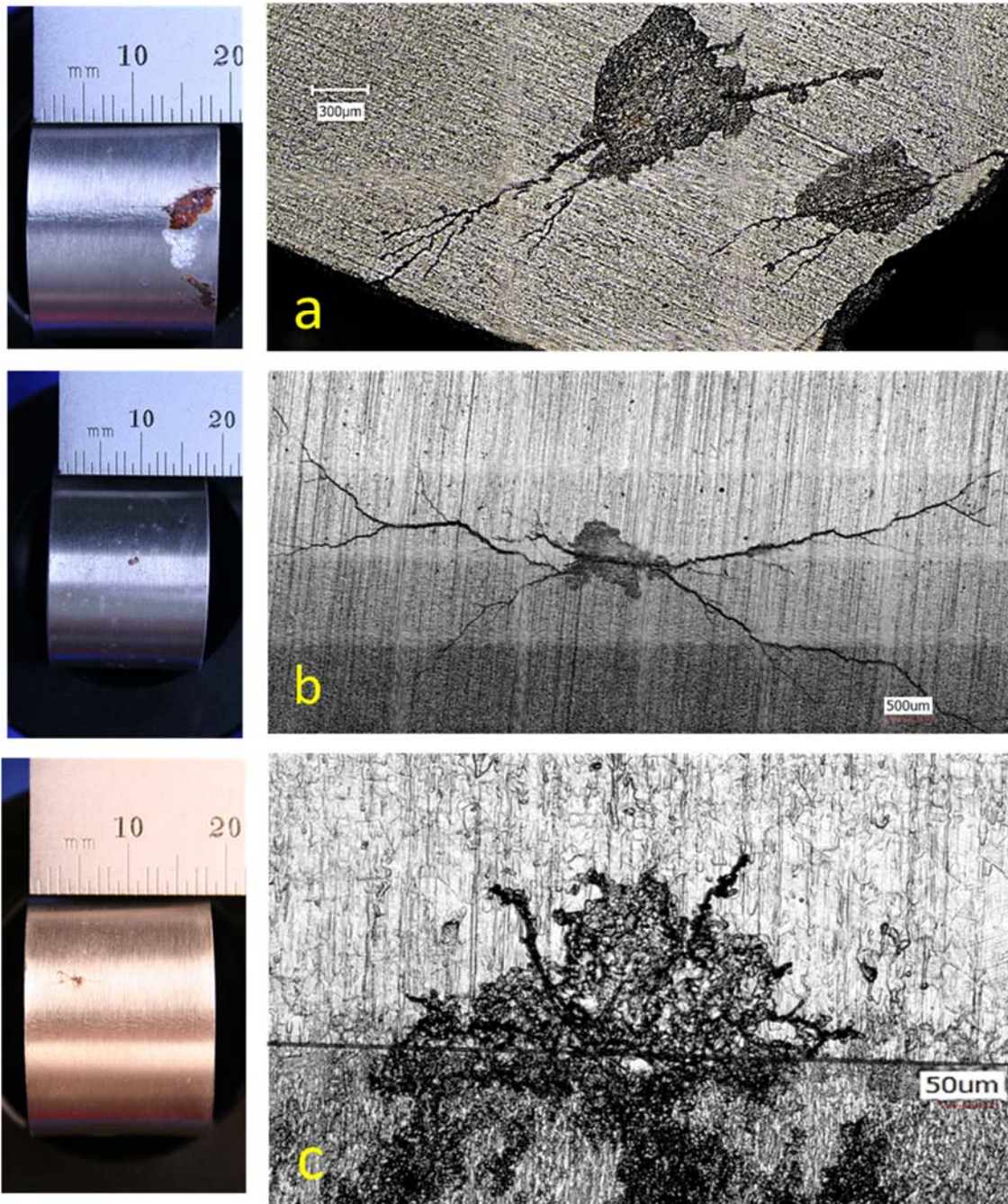


Figure 34. LCM images of cracking initiated on the surface of teardrop coupons at 50 °C and 50% RH for 100% sea salt (a), 25% sea salt + 75% CeO₂ (b), and at autogenous weld interface (shown by a dark line) in 25% sea salt + 75% artificial dust (c)

The entire surface of each 304L teardrop coupon in dehydrated sea salt under 50 °C and 50% RH for 3 months was carefully characterized. The areas of interest were sectioned for metallography analysis. Figure 35 is a composite image showing the pitting and cracking at various locations in the teardrop coupons. Again, a correlation between the pit size and the stress corrosion crack depth (length) cannot be established in these 304L teardrop coupons.

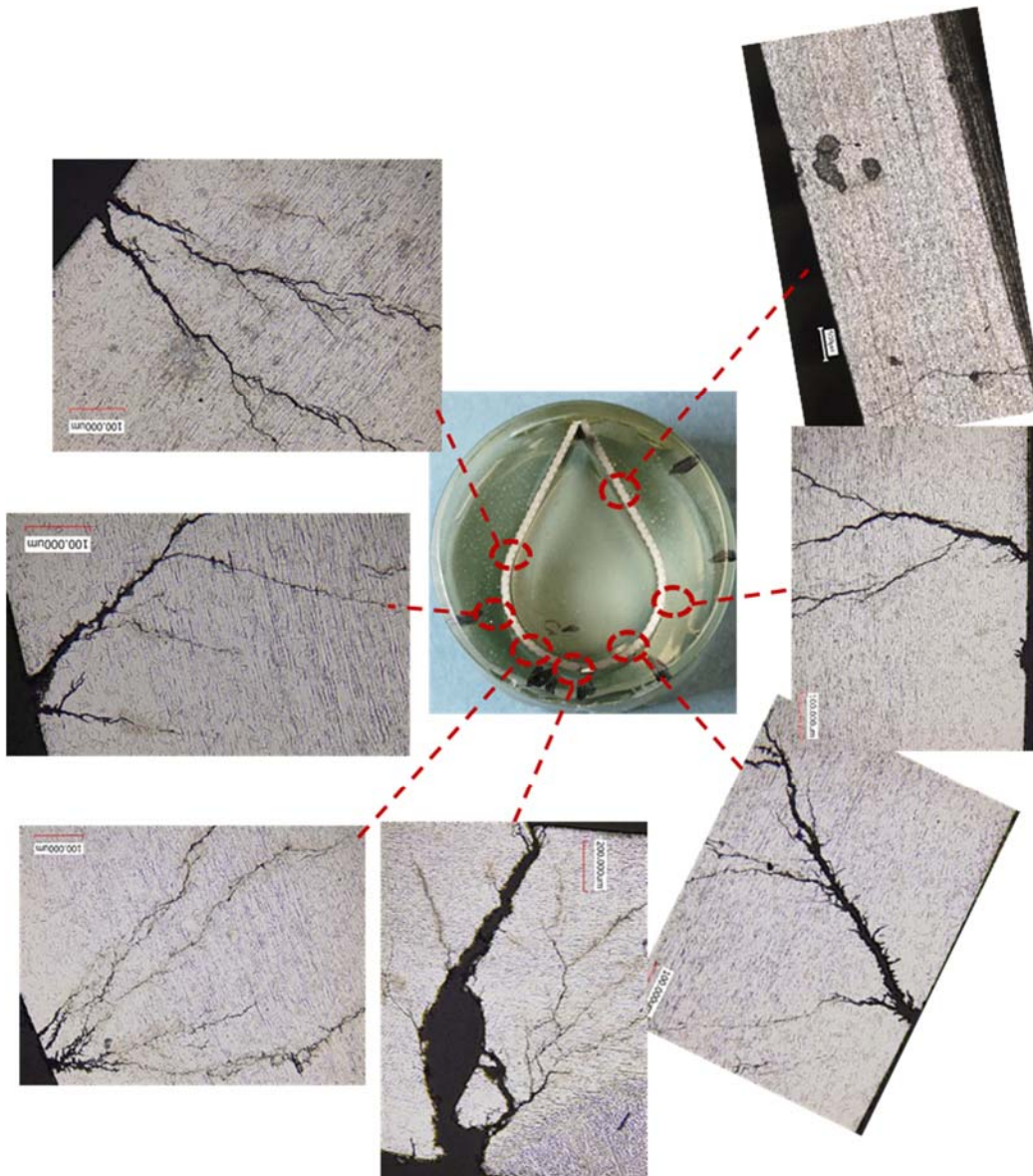


Figure 35. Composite image showing pitting/cracking at various locations in teardrop coupons exposed to dehydrated sea salt after 3-month exposure at 50 °C and 50% RH

4. LARGE PLATE DEMONSTRATION OF CISCC

The material resistance to CISCC in terms of CGR and threshold stress intensity factor (K_{ISCC}) can be determined by the bolt-load CT or the standard CT tests as discussed in Section 2. For non-stress relieved vessels subject to WRS loading in corrosive environments, such as the high-level nuclear waste tanks, large plate tests were carried out to demonstrate the cracking behavior on the structural level [35-37]. In the present case, the likelihood of CISCC during long-term storage of the SNF canisters is investigated by using a large stainless steel plate (dual certified 304/304L, Table 2) obtained from the same full-size mockup canister where the bolt-load CT specimens were harvested from (Section 2.3). This plate was sectioned through a region of the canister that contains a circumferential weld and has a planar dimension of 51×46 cm with a thickness of 16 mm and its weight is about 30 kg (see Figure 36). The size of the sectioned plate was carefully determined from a series of finite element calculations to minimize the redistribution or relieving of WRS due to cutting [38]. In a separate study by Wang et al. [39], neutron diffraction was used to determine the remaining WRS in a similar but smaller plate, which was also cut from the same mockup canister but contains an axial weld. Their experimental data confirmed that most of the as-welded residual stresses were retained in the sectioned plate. Therefore, it is reasonable to assume that the residual stresses in the large SRNL plate would be similar to those reported by Enos and Bryan (experiment) [15] and by Gim (finite element analysis) [32].

4.1. Starter Cracks

Starter cracks (aka seed cracks or machined cracks), have been introduced to the large plate in the weld region by EDM and are currently being exposed to a CISCC environment in 75% RH at room temperature since May 2019. The assumption of this demonstration is that the plate has existing stress corrosion cracks that have already initiated, and the unknown incubation time of crack initiation is ignored. Therefore, the objective of the demonstration is to verify the potential for continual crack growth as well as the crack growth characteristics (such as direction and branching, etc.); and if possible, to quantify the averaged CGR. Sensors, such as traditional ultrasonic test (UT), phased array ultrasonic test (PAUT), or other NDE techniques, may be used to detect and characterize crack growth.

There are seven starter cracks machined into the large plate (Figure 36), which contains a canister circumferential weld. The designations and descriptions of these EDM starter cracks are:

- (a) VT1, VT2: through-wall crack across the weld, crack length= 25 mm;
- (b) HT1: through-wall crack parallel to the weld edge, crack length= 12 mm;
- (c) VP1, VP2, VP3: semi-circular part-through-wall crack (surface crack) perpendicular to the weld edge, crack length= 12 mm and crack depth= 6 mm;
- (d) HP1: semi-circular part-through-wall crack (surface crack) parallel to the weld edge, crack length= 12 mm and crack depth= 6 mm.

The EDM crack configurations for types (a) to (d) above are shown in Figure 37. When these cracks are overlaid on the contour map of the residual stress parallel to the circumferential weld [15], the conceptual loading (WRS) of these cracks can be seen in Fig. 38. The starter crack tips are located in the weld/HAZ region.

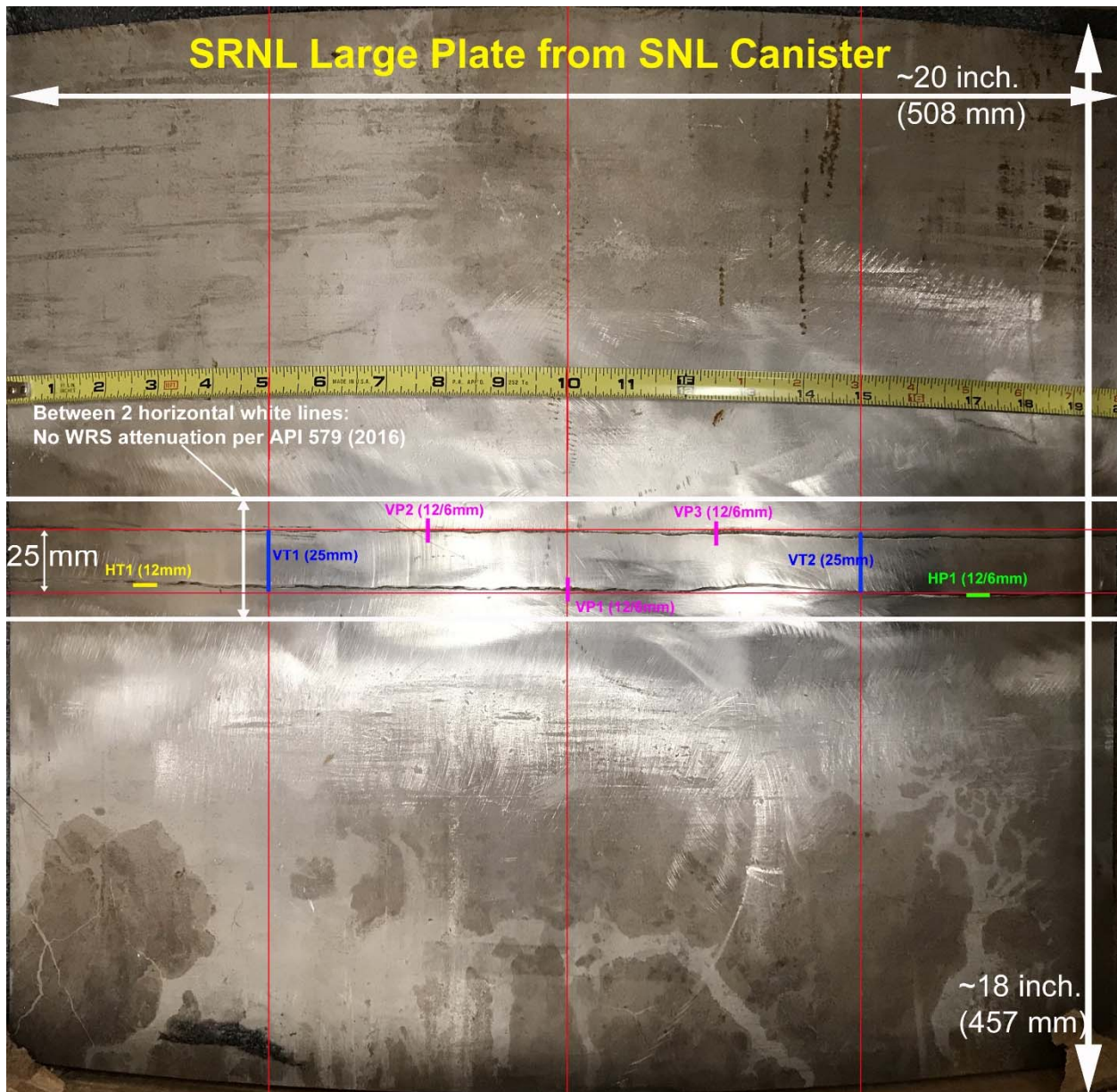


Figure 36. Large plate cut from a canister with an as-fabricated circumferential weld and the locations of starter cracks for CISCC test

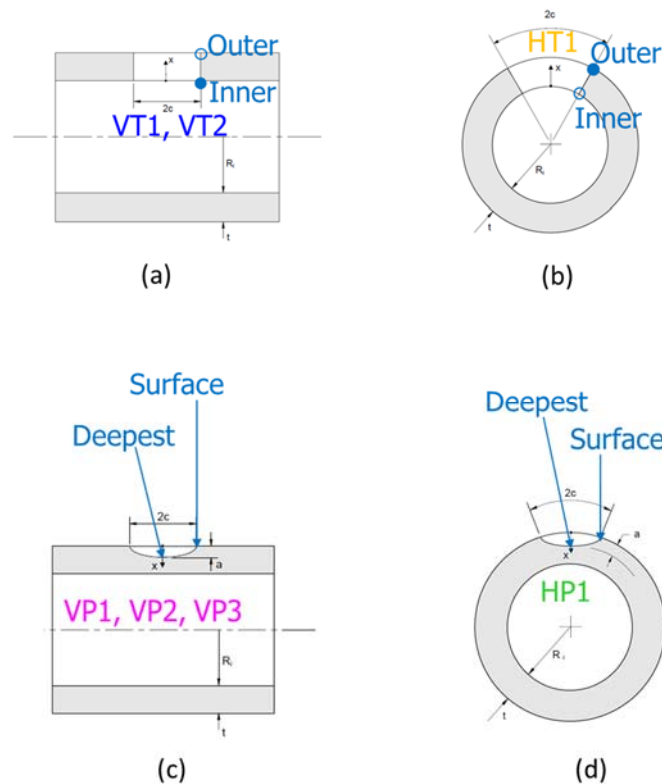


Figure 37. Large plate starter crack configurations: (a) VT1, VT2: through-wall crack across the weld; (b) HT1: through-wall crack parallel to the weld edge; (c) VP1, VP2, VP3: semi-circular part-through-wall crack perpendicular to the weld edge; (d) HP1: semi-circular part-through-wall crack parallel to the weld edge

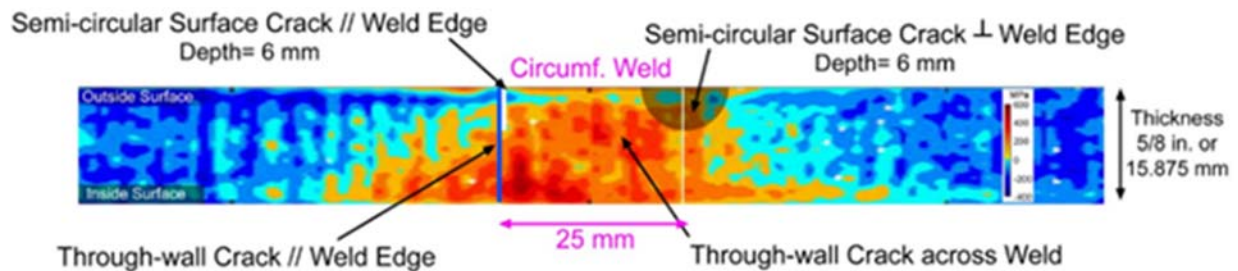


Figure 38. Large plate starter crack design as viewed from plate cross-section through the circumferential weld (superimposed over the contour map for welding residual stress parallel to the weld [15])

The through-wall cracks (VT1, VT2, and HT1) were fabricated with EDM wires of 0.25 mm (0.010 in.) diameter (65% copper and 35% zinc). The resulting width (burn gap) on the plate surface (corresponding to the outer surface of the canister) is approximately 0.43 mm by measurement. For the semi-circular, part-through-wall cracks (VP1, VP2, VP3, and HP1),

graphite ram EDM electrodes with width 0.51 mm (0.02 in.) were used. The machined seed crack width on the plate surface is about 0.81 mm.

4.2. Experiment

Artificial sea salt was prepared by following the procedure recommended by ASTM D1141, then deposited on the outer surface of the plate in the welded region with an air brush. The estimated salt load on the plate top surface was 2.35 g/m² chloride (dry). The salt coating procedure, as outlined in ASTM G41, “Standard Practice for Determining Cracking Susceptibility of Metals Exposed under Stress to a Hot Salt Environment,” was used to create an evenly distributed salt layer over the plate surface. Figure 39 shows the large plate after salt spray and drying.



Figure 39. Large plate with EDM starter cracks after salt spray and drying

A transparent polycarbonate (LEXAN™) box (enclosure) with an outside dimension of 56×53×15 cm with wall thickness 12.7 mm (0.5 in.) was constructed to house the large stainless steel plate which is supported by a riser over a salt bed with saturated NaCl. Based on ASTM E104, a constant 75% RH environment will be maintained inside the water-tight enclosure at room temperature.

Currently, seven PAUT wedges and transducers were mounted on the salt-free surface of the plate (or the concave side of the plate corresponding to the inner surface of the canister), as schematically shown in Figure 40. These sensors were positioned for *in-situ* detection of CISCC and CGR measurement when cracking occurs. It was designed for on-line monitoring without disturbing the exposure environment inside the polycarbonate enclosure. The plate may be temporarily removed from the enclosure for detailed NDE as needed. Figure 41 illustrates the overall experimental setup.

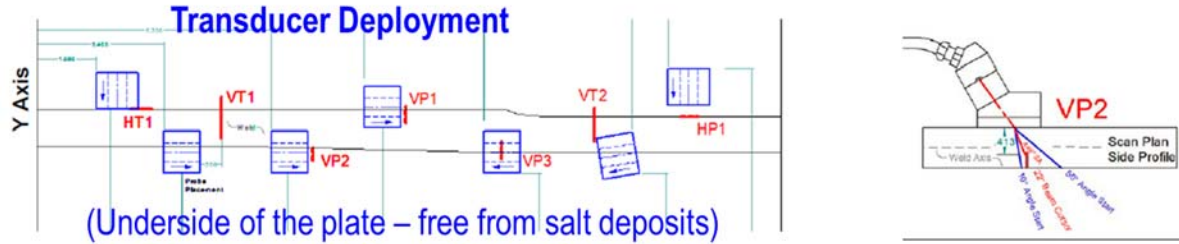


Figure 40. Phased array ultrasonic test (PAUT) for on-line monitoring of CISC in the large plate with 7 EDM starter cracks

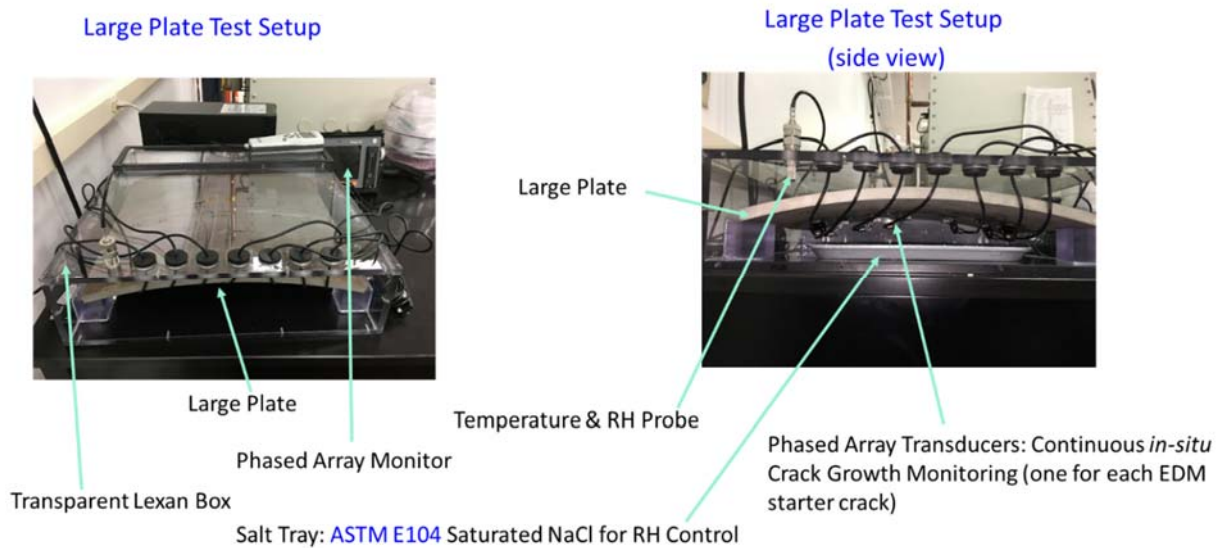


Figure 41. Experimental setup of the large plate CISC test under naturally deliquescing sea salt at room temperature and 75% RH

4.3. Experimental Observation

The test was initiated on May 8, 2019. The temperature and RH reached equilibrium quickly. In a few hours, numerous liquid droplets were observed on the top surface of the test plate. The close-up image near the starter crack VT1 is shown in Figure 42. To verify that this is indeed the naturally deliquescing condition rather than water vapor condensation, two separate small stainless steel coupons were inserted inside the polycarbonate enclosure on top of the large plate but remote from the weld: one coupon was treated with salt spray and drying using exactly the same procedure as preparing the large plate for test; and the other coupon was clean and free from dry salt deposit. Like the large plate, the small coupon with dry salt developed liquid droplets on the surface, but the other (clean) coupon looked dry (see Figure 43). Therefore, it can be concluded that this may be indeed a deliquescence phenomenon on metal surface rather than water vapor condensation. Although “liquid film” condition was originally expected but

had not observed, it may be possible that micro-droplets would form on the plate surface along with the more visible liquid droplets. This speculation cannot be verified with unaided eyes.

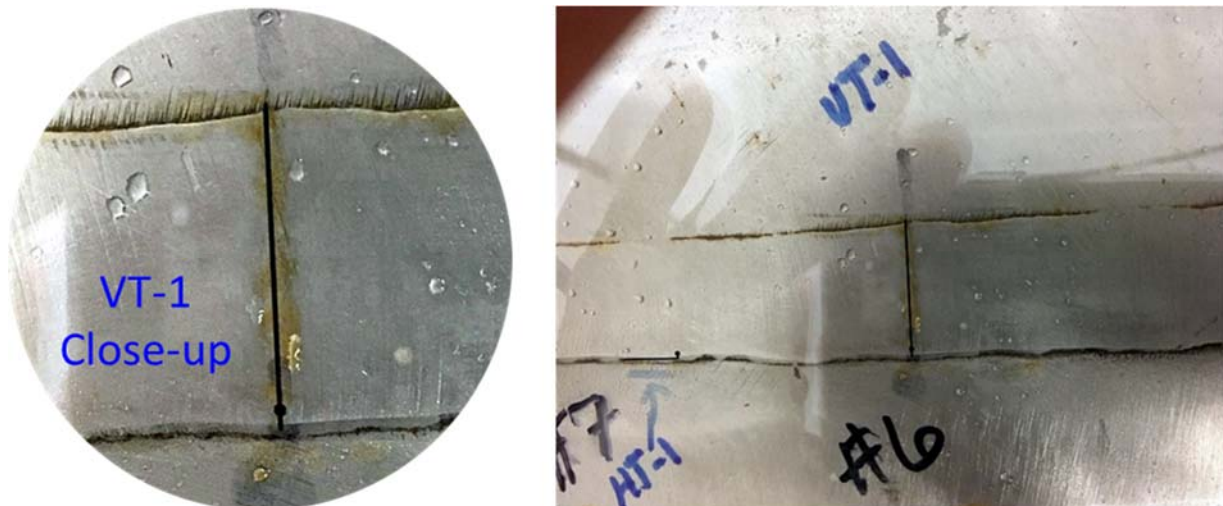


Figure 42. Deliquescence occurred in hours and forming numerous liquid droplets

The large plate test has been periodically examined and the starter cracks have been documented with digital images for searching evidence of SCC. The evolution of the starter cracks and their immediate vicinities, observed from May 9 to August 1, 2019, is shown in Figure 44. It can be seen that the general corrosion is progressively developed, especially along the weld and the base metal interface. No cracking has been observed so far.



Figure 43. Stainless steel coupons used to verify deliquescence phenomenon

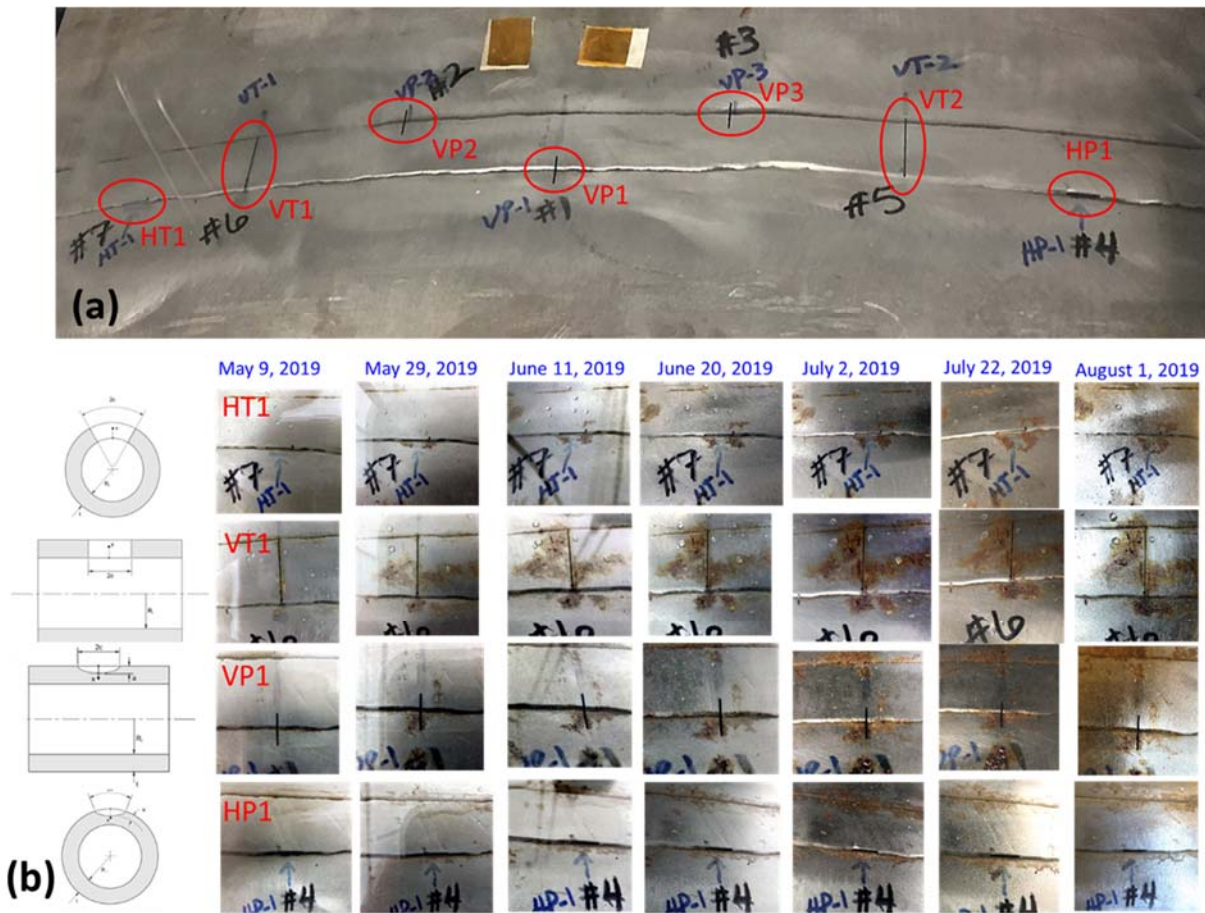


Figure 44. Layout and designations of EDM starter cracks (a) and evolution of chloride-induced corrosion near these cracks (b) during 3-month exposure at room temperature and 75% RH

4.4. Calculation of Stress Intensity Factors for Starter Cracks in Large Plate

Mode I stress intensity factor (K_I) is usually calculated to provide insight for the tendency of crack propagation. For the current large plate testing, K_I has been evaluated for each starter crack (Figures 36-39) under WRS loading. Korea University, under the I-NERI [18.1] joint project, used API 579 Fitness-for-Service procedure (2007) [24], to obtain the stress intensity factor solutions [25]. The general procedure of the calculation can be described as: (1) perform a 4th-order polynomial curve fitting according to Eq. 3 for the WRS (σ) measured by Sandia National Laboratories [15]; and then (2) calculate the stress intensity factor (K_I) based on the formulation provided by APT 579 [24]:

$$\sigma(x) = \sigma_0 + \sigma_1 \left(\frac{x}{t}\right) + \sigma_2 \left(\frac{x}{t}\right)^2 + \sigma_3 \left(\frac{x}{t}\right)^3 + \sigma_4 \left(\frac{x}{t}\right)^4 \quad (3)$$

where σ_i ($i=0$ to 4) are the coefficients of the 4th-order polynomial (Eq. 3), t is the canister wall thickness, and x is the through-wall coordinates with $x=0$ at either the outer surface or inner

surface, depending on the crack type (through-wall or part-through-wall) – see the coordinate system in Figures 37, 45-48, or its definition in API 579 [24].

Note that for the SRNL large plate testing with a circumferential canister weld (Figure 36), only the WRS parallel to the weld (RS2) and perpendicular to the weld (RS3) are relevant.

The K_I evaluation equation for each EDM starter crack and the corresponding WRS and its curve-fitting coefficients can be found from (i) to (iv) below. Both WRS measured at the weld centerline and at the HAZ were considered in calculation:

(i) Cylinder-Through-Wall Crack, Longitudinal Direction (VT1 and VT2 – see Figure 37 (a))

$$K_I = \left[\{ \sigma_m + p_c \} G_0 + \sigma_b (G_0 - 2G_1) \right] \sqrt{\pi c}$$

where σ_m is the membrane stress component, σ_b is the bending stress component, p_c is the crack face loading and is zero in the current large plate case, and the influence coefficients G_0 and G_1 are tabulated in API 579 [24].

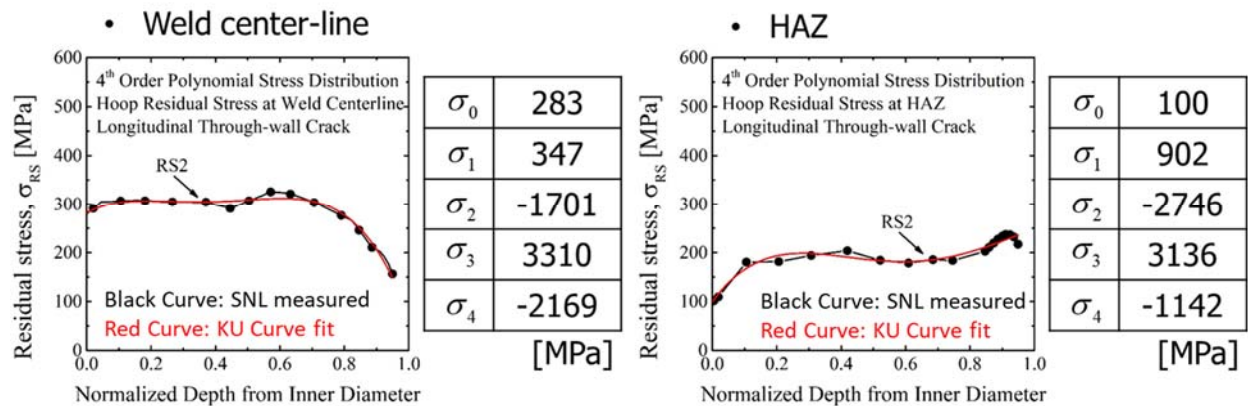


Figure 45. Curve-fitting of the welding residual stresses at weld centerline and at heat affected zone: WRS parallel to the circumferential weld: RS2; $x=0$ at the canister inner surface (Courtesy of Korea University under I-NERI/USA-ROK)

(ii) Cylinder-Surface Crack, Longitudinal Direction (VP1, VP2, and VP3 – see Figure 37 (c))

$$K_I = \left[G_0 (\sigma_0 + p_c) + G_1 \sigma_1 \left(\frac{a}{t} \right) + G_2 \sigma_2 \left(\frac{a}{t} \right)^2 + G_3 \sigma_3 \left(\frac{a}{t} \right)^3 + G_4 \sigma_4 \left(\frac{a}{t} \right)^4 \right] \sqrt{\frac{\pi a}{Q}}$$

Similar to (i), all symbols are defined in API 579 [24].

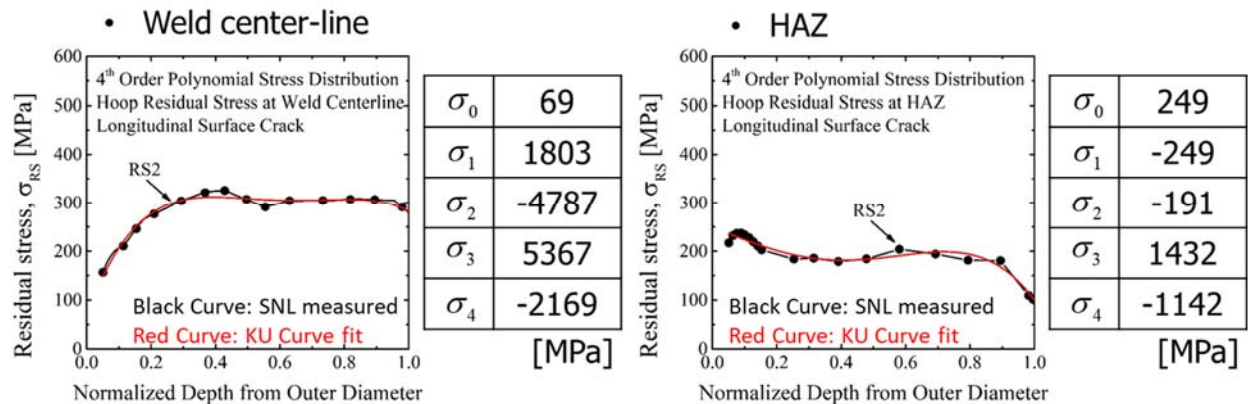


Figure 46. Curve-fitting of the welding residual stresses at weld centerline and at heat affected zone: WRS parallel to the circumferential weld: RS2; x= 0 at the canister outer surface (Courtesy of Korea University under I-NERI/USA-ROK)

(iii) Cylinder-Through-Wall Crack, Circumferential Direction (HT1 – see Figure 37 (b))

$$K_I = \left[\{ \sigma_m + p_c \} G_0 + \sigma_b (G_0 - 2G_1) \right] \sqrt{\pi c}$$

Similar to (i), all symbols are defined in API 579 [24].

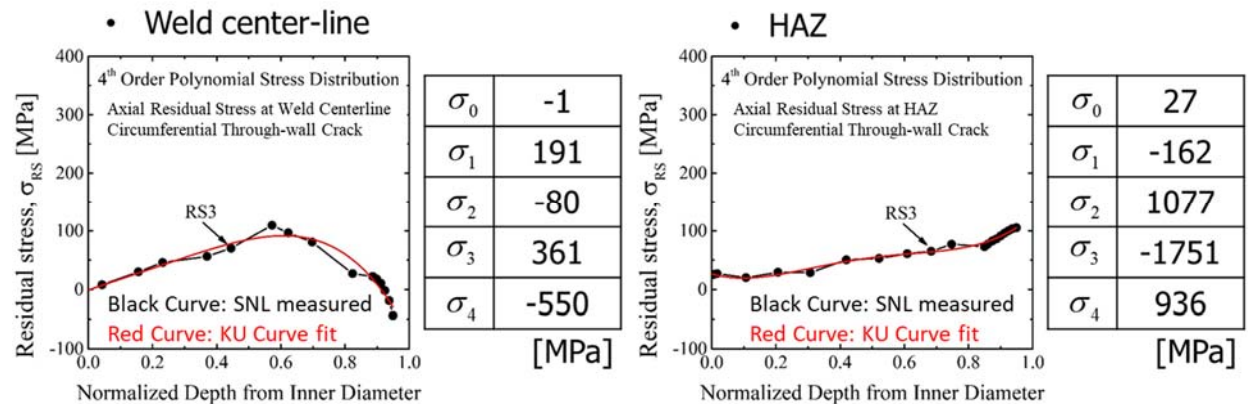


Figure 47. Curve-fitting of the welding residual stresses at weld centerline and at heat affected zone: WRS perpendicular to the circumferential weld: RS3; x= 0 at the canister inner surface (Courtesy of Korea University under I-NERI/USA-ROK)

(iv) Cylinder-Surface Crack, Circumferential Direction (HP1 - Figure 37 (d))

$$K_I = \left[G_0 (\sigma_0 + p_c) + G_1 \sigma_1 \left(\frac{a}{t} \right) + G_2 \sigma_2 \left(\frac{a}{t} \right)^2 + G_3 \sigma_3 \left(\frac{a}{t} \right)^3 + G_4 \sigma_4 \left(\frac{a}{t} \right)^4 \right] \sqrt{\frac{\pi a}{Q}}$$

Similar to (i), all symbols are defined in API 579 [24].

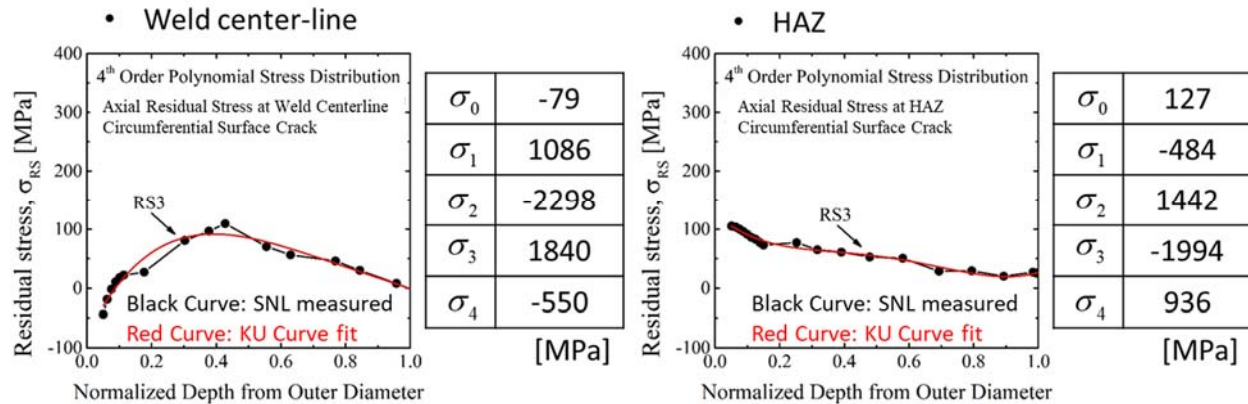


Figure 48. Curve-fitting of the welding residual stresses at weld centerline and at heat affected zone: WRS parallel to the circumferential weld: RS3; $x=0$ at the canister outer surface (Courtesy of Korea University under I-NERI/USA-ROK)

The calculation results from (i) to (iv) above are summarized in Figure 49 (where W.C.L. represents weld centerline). More specifically, the calculated K_I values for each of the starter crack are listed in Tables 7-10.

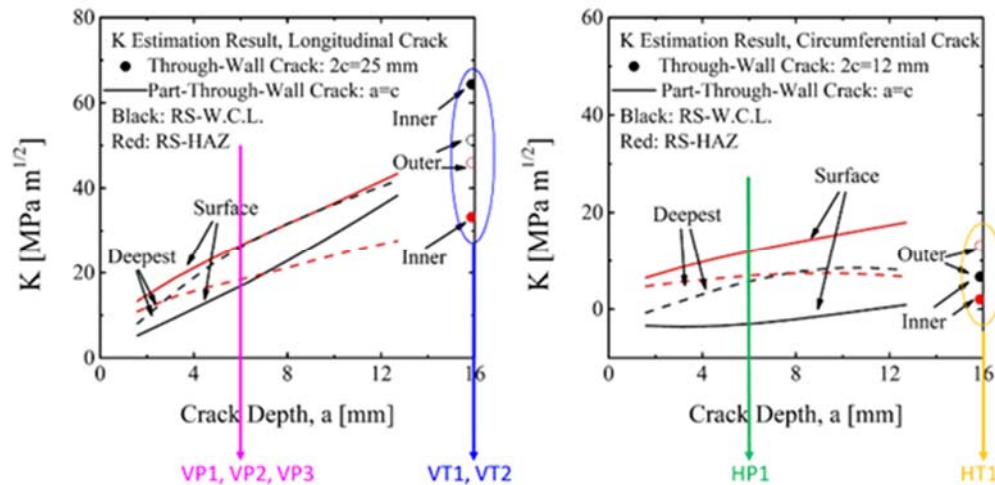


Figure 49. Stress intensity factors of the starter cracks in the residual stress fields for a circumferential weld in the mockup canister (Courtesy of Korea University under I-NERI/USA-ROK)

**Table 7. Stress Intensity factors for starter cracks VP1, VP2, and VP3
(Axial surface crack: $a = c = 6$ mm; semicircular)**

Welding Residual Stress	Crack Tip Location	Stress Intensity factor (MPa√m)
Weld Centerline	Deepest Point	26.0
	Surface Point	16.9
Heat Affected Zone	Deepest Point	18.3
	Surface Point	26.4

**Table 8. Stress Intensity factors for starter cracks VT1 and VT2
(Axial through-wall crack: $c = 12.5$ mm)**

Welding Residual Stress	Crack Tip Location	Stress Intensity factor (MPa√m)
Weld Centerline	Outside Surface	51.6
	Inside Surface	64.3
Heat Affected Zone	Outside Surface	46.1
	Inside Surface	33.3

**Table 9. Stress Intensity factors for starter crack HP1
(Circumferential surface crack: $a = c = 6$ mm; semicircular)**

Welding Residual Stress	Crack Tip Location	Stress Intensity factor (MPa√m)
Weld Centerline	Deepest Point	5.6
	Surface Point	-3
Heat Affected Zone	Deepest Point	7
	Surface Point	12

**Table 10. Stress Intensity factors for starter cracks HT1
(Circumferential through-wall crack: $c = 12$ mm; semicircular)**

Welding Residual Stress	Crack Tip Location	Stress Intensity factor (MPa√m)
Weld Centerline	Outside Surface	6.5
	Inside Surface	6.7
Heat Affected Zone	Outside Surface	13.3
	Inside Surface	1.9

A collection of field test data obtained on Miyakojima Island, Japan [4] is shown in Fig. 50. It can be seen that the SCC could take place at a load as low as $K_I = 1.0$ MPa√m. This implies that the K_{ISCC} of the canister materials exposed to marine environments could be lower than 1.0 MPa√m. Therefore, based on the calculation results in Fig. 49 and Tables 7-10, CISCC would occur in most of the starter cracks in the large plate if the as-fabricated WRS was not significantly altered or relieved by plate sectioning from the mockup canister and by machining for starter cracks by EDM.

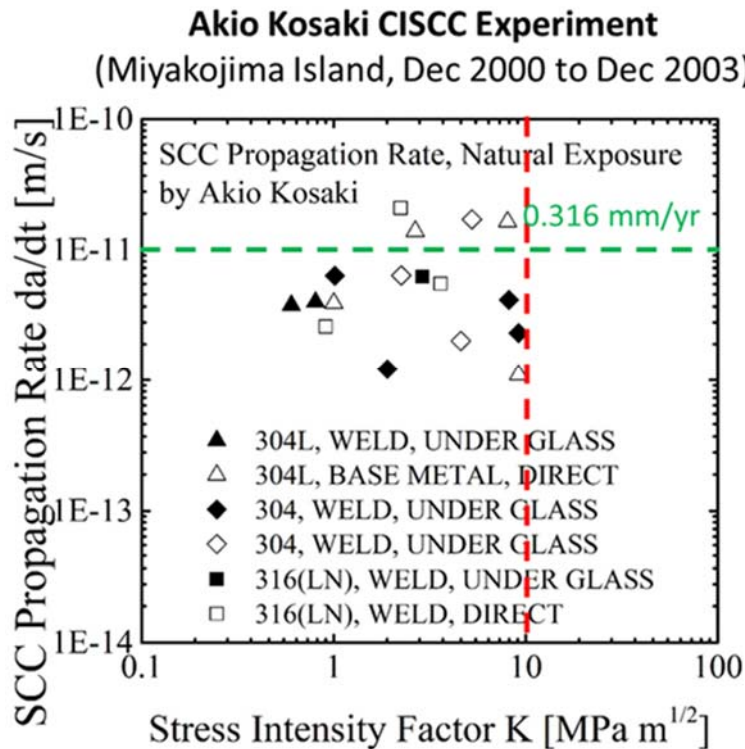


Figure 50. Summary of crack growth rate field test data obtained on Miyakojima Island [4]
(Courtesy of Korea University under I-NERI/USA-ROK)

5. CONCLUDING REMARKS

This report describes the experiments for the determination of chloride-induced stress corrosion crack growth rate using bolt-load compact tension specimens at 50 °C with 30% and 50% relative humidity (304 stainless steel in various salt/dust mixtures), and in nominally 75% relative humidity at room temperature and at 37 °C (dual certified 304/304L in artificial sea salt). The tests used the deliquescent nature of the dry salt and allowed the naturally formed brine to interact with the naturally sharp crack front (crack tip) created by mechanical fatigue pre-cracking according to ASTM E1681 recommendations. This report also includes recent results of crack growth rates obtained at Korea University through I-NERI/USA-ROK joint project by using immersion test in 5% salinity solution at 50 °C with standard compact tension specimens specified by ASTM E1820. All test results reported here are consistent with the prediction from a straight regression line in a semi-logarithmic plot (Fig. 19), which was obtained from a very large database [17-19] for stainless steels under wide range of chloride-induced stress corrosion cracking environments. It appears that this simple form of crack growth rate (Section 2.3.2, Eq. 2) could support the development of ASME BPV Section XI Code Case N-860 in the application of a crack growth rate after a CISCC flaw has been detected by inservice inspection [2].

A large plate (approximately 51×46 cm) has been sectioned from a full-size mockup canister [15] in a region containing a circumferential weld. Starter cracks were fabricated by EDM in the weld region of the plate. It is used to demonstrate stress corrosion cracking under naturally deliquescing condition of dry salt in 75% relative humidity at room temperature. Phased array sensors were deployed on the large plate for on-line monitoring of stress corrosion crack growth. In addition, periodic examination of the plate is also planned by using other NDE techniques. Based on stress intensity factor calculations, the starter cracks are expected to grow, provided that the as-fabricated welding residual stress was not significantly altered or redistributed by plate sectioning from the mockup canister and by EDM of the starter cracks. The large plate test is currently in progress since May 2019. Active general corrosion has been observed in the vicinity of each crack but the stress corrosion cracking has not taken place.

6. REFERENCES

- [1] NRC Regulations, Title 10, Code of Federal Regulations, Part 72 (10 CFR 72) - Licensing Requirements for The Independent Storage of Spent Nuclear Fuel, High-Level Radioactive Waste, and Reactor-Related Greater Than Class C Waste, Subpart 72.42 “Duration of license; renewal,” U. S. Nuclear Regulatory Commission, Washington DC, UAS.
- [2] Broussard, J., Bryan, C., Sindelar, R., and Lam, P. S., 2019, “Crack Growth Rate Model for CISCC of Stainless Steel Canisters,” Paper No. PVP2019-94055, Proceedings of ASME Pressure Vessels and Piping Conference, San Antonio, Texas, USA.
- [3] Kosaki, A., 2005, “The corrosion behavior of one-fifth scale lid models of transport cask submerged in sea bottom,” *Corrosion Science*, 47, pp. 2361–2376.
- [4] Kosaki, A., 2006, “SCC Propagation Rate of Type 304, 304L Steels under Oceanic Air Environment,” Paper No. ICONE14-89271, Vol. 1, Plant Operations, Maintenance and Life Cycle; Component Reliability and Materials Issues; Codes, Standards, Licensing and Regulatory Issues; Fuel Cycle and High Level Waste Management, International Conference on Nuclear Engineering, July 17-20, Miami, Florida, USA, pp. 443-450
- [5] Tani, J., Mayuzumi, M., Arai, T., and Hara, N., 2007, “Stress Corrosion Cracking Growth Rates of Candidate Canister Materials for Spent Nuclear Fuel Storage in Chloride-Containing Atmosphere,” *Materials Transactions*, Vol. 48, No. 6, pp. 1431 to 1437.
- [6] Kosaki, A., 2008, “Evaluation method of corrosion lifetime of conventional stainless steel canister under oceanic air environment,” *Nuclear Engineering and Design*, 238, pp. 1233–1240.
- [7] Tani, J., Mayuzumi, M., and Hara, N., 2008, “Stress corrosion cracking of stainless-steel canister for concrete cask storage of spent fuel,” *Journal of Nuclear Materials* 379, pp. 42–47.

- [8] Tani, J. I., 2009, "Initiation and Propagation of Stress Corrosion Cracking of Stainless Steel Canister for Concrete Cask Storage of Spent Nuclear Fuel," *Corrosion*, Vol. 65, No. 3, pp. 187-194.
- [9] Caseres, L. and Mintz, T. S., 2010, *Atmospheric Stress Corrosion Cracking Susceptibility of Welded and Unwelded 304, 304L, and 316L Austenitic Stainless Steels Commonly Used for Dry Cask Storage Containers Exposed to Marine Environments*, NUREG/CR-7030, Office of Nuclear Regulatory Research, U.S. Nuclear Regulatory Commission, Washington, D.C., USA.
- [10] Shirai, K., Tani, J., and Saegusa, T., 2011, *Study on Interim Storage of Spent Nuclear Fuel by Concrete Cask for Practical Use -Feasibility Study on Prevention of Chloride Induced Stress Corrosion Cracking for Type 304L Stainless Steel Canister*, CRIEPI N10035, Central Research Institute of Electric Power Industry, Tokyo, Japan (In Japanese).
- [11] Sindelar, R. L., Carter, J. T., Duncan, A. J., Garcia-Diaz, B. L., Lam, P. S., and Wiersma, B. J., 2016, "Chloride-Induced Stress Corrosion Crack Growth under Dry Salt Conditions – Application to Evaluate Growth Rates in Multipurpose Canisters," Paper No. PVP2016-63884, Proceedings of the ASME Pressure Vessels & Piping Conference, Vancouver, BC, Canada.
- [12] Duncan, A. J., Lam, P. S., Sindelar, R. L., and Carter, J. T., 2017, "Crack Growth Rate Testing with Instrumented Bolt-Load Compact Tension Specimens under Chloride-Induced Stress Corrosion Cracking Conditions in Spent Nuclear Fuel Canisters," Paper No. PVP2017-66105, Proceedings of the ASME Pressure Vessels & Piping Conference, Waikoloa, Hawaii, USA.
- [13] Duncan, A. J., Lam, P. S., Sindelar, R. L., and Metzger, K. E., 2018, "Crack Growth Rate Testing of Bolt-Load Compact Tension Specimens under Chloride-Induced Stress Corrosion Cracking Conditions in Spent Nuclear Fuel Canisters," Paper Number PVP2018-84753, Proceedings of the ASME Pressure Vessels & Piping Conference, Prague, Czech Republic.
- [14] Lam, P. S., Duncan, A. J., Ward, L. N., Sindelar, R. L., Kim, Y. J., Jeong, J. Y., Lee, H. J., and Lee, M. W., 2019, "Crack Growth Rate Testing and Large Plate Demonstration under Chloride-Induced Stress Corrosion Cracking Conditions in Stainless Steel Canisters for Storage of Spent Nuclear Fuel," Paper Number PVP2019-94031, Proceedings of the ASME Pressure Vessels & Piping Conference, San Antonio, Texas, USA.
- [15] Enos, D. G. and Bryan, C. R., 2016, *Final report: Characterization of Canister Mockup Weld Residual Stresses*, FCRD-UFD-2016-000064 Sandia National Laboratories, Albuquerque, New Mexico, USA.
- [16] Chu, S., 2014, *Flaw Growth and Flaw Tolerance Assessment for Dry Cask Storage Canisters*, Report 3002002785, EPRI, Palo Alto, California, USA

- [17] Ilgen, A., Bryan, C. and Hardin, E., 2015, *Draft Geologic Disposal Requirements Basis for STAD Specifications*, FCRD-NFST-2013-000723 / SAND2015-2175R, Sandia National Laboratories, Albuquerque, New Mexico, USA
- [18] Bryan, C., Dingreville, R., Enos, D., 2016, *Weld Residual Stress Final Results and CISCC Model Development*, EPRI Extended Storage Collaboration Program (ESCP) Meeting, November 29, 2016, Charlotte, North Carolina, USA
- [19] Bryan, C. and Enos, D., 2016, *Summary of available data for estimating chloride-induced SCC crack growth rates for 304/316 stainless steel*, SAND2016-2992R, Sandia National Laboratories, Albuquerque, New Mexico, USA
- [20] Lam, P. S. and Kim, Y. J., 2016, I-NERI Project Number 2016-001-K: *Flaw Stability and Stress Corrosion Cracking of Austenitic Stainless Steel Canisters for Long Term Storage and Transportation of LWR Used Fuel*, U. S. Department of Energy - Office of Nuclear Energy, Washington D. C., USA.
- [21] Jeong, J. Y., Lee, M. W., Kim, Y. J., Sindelar, R., and Duncan, A., 2019, "Development of an apparatus for chloride induced stress corrosion cracking test using immersion method with constant displacement condition," Paper No. PVP2019-93922, Proceedings of ASME Pressure Vessels and Piping Conference, San Antonio, Texas, USA.
- [22] Jeong, J. Y. and Kim, Y. J., 2019, "Development of a Tester for Accurate Measurement of Chloride Induced Stress Corrosion Crack Growth Rate," in preparation for publication.
- [23] Metzger, K. E., Hair, K. N., Duncan, A. J., Martinez-Rodriguez, M. J., and Garcia-Diaz, B. L., 2017, "CISCC of Stainless Steel Under Natural Deliquescence of Salt/Dust Mixtures," 2017 American Nuclear Society (ANS) Winter Meeting and Nuclear Technology Expo, Washington, D. C., USA.
- [24] API 579-1/ASME FFS-1, 2007, *Fitness-For-Service (API 579 Second Edition)*, American Petroleum Institute, Washington, DC., USA.
- [25] Lee, H. J., Kim, Y. J., Lam, P. S., and Sindelar, R. L., 2019, "Engineering J estimates for Spent Fuel Canisters under Combined Mechanical and Welding Residual Stresses," Paper Number PVP2019-93936, Proceedings of the ASME Pressure Vessels & Piping Conference, San Antonio, Texas, USA, July 2019.
- [26] ASME Boiler and Pressure Vessel Code, Section XI, *Rules for Inservice Inspection of Nuclear Power Plant Components*, 2017, American Society of Mechanical Engineers, New York, NY., USA.
- [27] Sedriks, A. J., 1990, *Corrosion Testing Made Easy: Stress Corrosion Cracking Test Methods*, NACE International (National Association of Corrosion Engineers), Houston, TX, USA.
- [28] Strainsert Company, West Conshohocken, PA, USA (<https://www.strainsert.com>)

- [29] Lam, P. S., Zapp, P. E., Duffey, J. M., Dunn, K. A., 2009, "Stress Corrosion Cracking in Tear Drop Specimens," PVP2009-77432, Proceedings of the ASME 2009 Pressure Vessels and Piping Division Conference, Prague, Czech.
- [30] Zapp, P. E., Duffey, J. M., Lam, P. S., Dunn, K. A., Veirs, D. K., Worl, L. A., and Berg, J. M., 2010, "Relative Humidity and the Susceptibility of Austenitic Stainless Steel to Stress Corrosion Cracking in an Impure Plutonium Oxide Environment," *Journal of Nuclear Materials Management*, Vol. XXXVIII, No. 3, pp. 4-14.
- [31] Enos, D. G., Bryan, C. R., and Norman, K. M., 2013, *Data Report on Corrosion Testing of Stainless Steel SNF Storage Canisters*, FCRD-UFD-2013-000324, SAND2013-8314P, Sandia National Laboratories, Albuquerque, NM, USA
- [32] Gim, J. M., Kim, J. S., Kim, Y. J., and Lam, P. S., 2018, "FE welding residual stress analysis and validation for spent nuclear fuel canisters," Paper Number PVP2018-84857, Proceedings ASME Pressure Vessels & Piping Conference, Prague, Czech Republic.
- [33] Endo/Tech™, Halifax, Canada (<https://endo-tech-com.3dcartstores.com/>)
- [34] Mickalonis, J. I. and Duffey, J. M., 2014, *SRNL Shelf Life Studies – SCC Studies at Room Temperature*, SRNL-STI-2014-00418, Savannah River National Laboratory, Aiken, SC, USA
- [35] Lam, P. S., Chang, C., Chao, Y. J., Sindelar, R. L., Stefek, T. M., and Elder III, J. B., 2005, "Stress Corrosion Cracking of Carbon Steel Weldments," Paper Number PVP2005-71327, Proceedings of ASME Pressure Vessels and Piping Conference, Denver, Colorado, USA.
- [36] Lam, P. S., 2009, *Investigation of the Potential for Caustic Stress Corrosion Cracking of A537 Carbon Steel Nuclear Waste Tanks*, SRNS-STI-2009-00564 Rev.1, Savannah River Nuclear Solutions, Aiken, South Carolina, USA.
- [37] Lam, P. S., Stripling, C. S., Fisher, D. L., and Elder III, J. B., 2010, "Potential for Stress Corrosion Cracking of A537 Carbon Steel Nuclear Waste Tanks Containing Highly Caustic Solutions," Paper No. PVP2010-25117, Proceedings of ASME Pressure Vessels and Piping Conference, Bellevue, Washington, USA.
- [38] Bryan, C. to Sindelar, R. L., email communication, August 14, 2018.
- [39] Wang, J. A., Payzant, A., Bunn, J., and An, K., 2018, *Neutron Residual Stress mapping for Spent Nuclear Fuel Storage Canister Weldment*, ORNL/TM-2018/827, Oak Ridge, Tennessee, USA.